www.sciencemag.org/cgi/content/full/science.1238477/DC1

Supplementary Materials for

Recurrent Insect Outbreaks Caused by Temperature-Driven Changes in System Stability

William A. Nelson,* Ottar N. Bjørnstad,[2] Takehiko Yamanaka

*Corresponding author. E-mail: nelsonw@queensu.ca

Published 1 August 2013 on *Science* Express
DOI: 10.1126/science.1238477

This PDF file includes:

Supplementary Text

Model development and parameterization

Here we develop a population model for holometabolic insects with intraspecific larval competition and temperature-dependence in their birth, development and mortality rates. The life-history functions are developed and parameterized for the smaller tea tortrix *Adoxophyes honmai* using laboratory data on *A. honmai* and a closely related species *A. orana*. Model development follows the approach of Yamanaka *et al.* (*15*), which is based on the stage-structured formalism of Nisbet & Gurney (*31*). The resulting model is a set of coupled integro-delayed-differential equations that can be used to predict dynamics under both constant and seasonally driven temperature regimes. The insect life-cycle is described using the following stage-structure

$$\frac{dE(t)}{dt} = R_E(t) - R_L(t) - \delta_E(t)E(t) \tag{1}$$
$$\frac{dL(t)}{dt} = R_L(t) - R_P(t) - \delta_L(t)L(t) \tag{2}$$
$$\frac{dP(t)}{dt} = R_P(t) - R_A(t) - \delta_P(t)P(t) \tag{3}$$
$$\frac{dA(t)}{dt} = R_A(t) - R_S(t) - \delta_A(t)A(t) \tag{4}$$
$$\frac{dA_S(t)}{dt} = R_S(t) - \delta_{A_S}(t)A_S(t) \tag{5}$$

where $E(t)$ is egg abundance, $L(t)$ is larvae abundance, $P(t)$ is pupal abundance, $A(t)$ is non-senescent adult abundance, and $A_S(t)$ is senescent adult abundance at time t. The senescence stage is motivated by survivorship curves (*32*), which show low adult mortality for a period of time, followed by a substantially higher mortality rate and a concomitant cessation of reproduction. The per capita mortality rates for stage i are denoted by $\delta_i(t)$, and stage-specific recruitment rate by $R_i(t)$. Recruitment rates are given by

$$R_E(t) = b(t)A(t) \tag{6}$$
$$R_L(t) = R_E(t - \tau_E(t))S_E(t)\frac{h_E(t)}{h_E\left(t - \tau_E(t)\right)} \tag{7}$$
$$R_P(t) = R_L(t - \tau_L(t))S_L(t)\frac{h_L(t)}{h_L\left(t - \tau_L(t)\right)} \tag{8}$$
$$R_A(t) = R_P(t - \tau_P(t))S_P(t)\frac{h_P(t)}{h_P\left(t - \tau_P(t)\right)} \tag{9}$$
$$R_S(t) = R_A(t - \tau_A(t))S_A(t)\frac{h_A(t)}{h_A\left(t - \tau_A(t)\right)} \tag{10}$$

where $\tau_i(t)$ is the duration of the ith stage for individuals that enter the stage at time t, $S_i(t)$ is through-stage survival, $h_i(t)$ is the development rate, and $b(t)$ is the per-capita birth rate. Following

(*31*), stage durations are given by the solution to the following implicit equations

$$1 = \int_{t-\tau_E(t)}^{t} h_E(\xi)d\xi \tag{11}$$

$$1 = \int_{t-\tau_L(t)}^{t} h_L(\xi)d\xi \tag{12}$$

$$1 = \int_{t-\tau_P(t)}^{t} h_P(\xi)d\xi \tag{13}$$

$$1 = \int_{t-\tau_A(t)}^{t} h_A(\xi)d\xi \tag{14}$$

and stage survivorships are given by

$$S_E(t) = \exp\left(-\int_{t-\tau_E(t)}^{t} \delta_E(\xi)d\xi\right) \tag{15}$$

$$S_L(t) = \exp\left(-\int_{t-\tau_L(t)}^{t} \delta_L(\xi)d\xi\right) \tag{16}$$

$$S_P(t) = \exp\left(-\int_{t-\tau_P(t)}^{t} \delta_P(\xi)d\xi\right) \tag{17}$$

$$S_A(t) = \exp\left(-\int_{t-\tau_A(t)}^{t} \delta_A(\xi)d\xi\right) \tag{18}$$

The laboratory data (detailed below) suggests that temperature dependence for all life-history rates of *A. honmai* (*32*, *33*) and the closely related species *A. orana* (*34*, *35*) can be described using an exponential function of the form ae^{bD}, which relates daily temperature D to stage-specific life-history rates. The advantage of having temperature-dependent data on two species for many of the life-history traits is that it lends a degree of generality to the functional forms and parameter estimates. To evaluate the potential sensitivity of our conclusions to the particular strain used in the laboratory experiments (or species for that matter), we perform our model analyses across a wide range of parameter space (see *Stability analysis under constant temperature*).

There is strong statistical support for allowing each stage i and each life-history trait j to have a different intercept parameter (a_{ij}), but for most to share the same slope parameter (b). The exception is *winter mortality*, which we describe separately. Table S1 shows the comparison among statistical models, and Table S2 shows the estimates for all parameters. Note that we have studied the top three models in Table S2 and our results are robust to assumptions of how b is aggregated. However, the exact location of the Hopf bifurcation shifts somewhat with the parameterization (see *Stability analysis under constant temperature*). For clarity, we redefine the stage-specific life-history functions for development ($h_i(t)$), birth ($b(t)$) and warm temperature mortality rates ($g_i(t)$) as

$$h_i(t) = \alpha_i e^{\beta D(t)} \tag{19}$$
$$b(t) = b_o e^{\beta D(t)} \tag{20}$$
$$g_i(t) = d_i e^{\beta D(t)} \tag{21}$$

For development rates, there is good quality data for both species (Fig. S1). We define the transition between non-senescent and senescent adults by the 50th mortality percentile. Based on Nabeta *et al.* (*32*), this transition corresponds well with the oldest age of reproduction, so we assume only non-senescent adults contribute to reproduction. The birth rate data is more variable between the two species compared to development rates, but both species show a clear increasing response to higher temperature (Fig. S2). Mortality rates are similarly more variable than development rates, but there is a consistent increase with temperature that is well described by an exponential function (Fig. S3). We refer to these as warm temperature mortality rates to distinguish them from the distinct impact that cold temperatures have on mortality rates (discussed below). Again, we guard against potential sensitivity to differences between the two species in our parameter estimates by analyzing the model across a wide range of parameter space.

The life-history rate functions describing birth, development and mortality (Eqns. 19-21) do not include effects of high temperature beyond the temperature optimum, such as the sharp drop-off in development rates observed for insects at high temperatures (*36*). For our study, there is no need to include such high-temperature effects because over 99% of the observed temperature data fall below 30°C, which is the upper temperature in the laboratory data. However, the negative effects of high-temperature would need to be studied in the laboratory and incorporated in the life-history rate functions if the model was to be used to predict dynamics for settings where the temperature exceeded 30°C, such as when studying the potential impact of climate warming. As observed in a wide range of insects (*37*), we assume that development rates decrease smoothly as temperature drops below the lowest temperature observed in the laboratory.

In addition to warm temperature mortality (temperature above freezing), there is an abundance of anecdotal evidence indicating that mortality rates increase dramatically as temperature decreases, and that this is different among stages with the larval stage being much less resistant to cold temperature (temperature below 0° C). There is no diapause stage in *A. honmai* (*14*), which means that winter survivorship can be described by temperature-dependent mortality rates. To incorporate cold temperature mortality, we add an additional mortality term as $g_W(t) = d_W e^{-\beta_W D(t)}$, where d_W is the winter mortality scalar and β_W is the slope parameter. The only available data available is from Jo & Kim (*38*) where different stages of the moths were exposed to -5, -10 and -15°C for 0, 2, 4 and 8hrs. Extrapolating those temperatures to 24hr exposure gives us a rough estimate of the daily mortality rate for subzero temperatures (Fig. S4). While the data is sparse, the evidence for larval stages suggests that an exponential function is not unrealistic. This helps simplify some of the model functions later on. We assume the parameters are the same for all stages, but evaluate the potential importance of stage-specific differences in the mortality scalar (d_W) by allowing for each stage to vary independently in the stability analysis.

We consider a situation where larval competition causes increased mortality rates (g_C), which is motivated by our previous work (*15*). Specifically, we assume $g_C(t) = d_C e^{\gamma_C D(t)} L(t)$, which allows that

the intensity of competition can change with temperature. Since we have no knowledge of how fast competition is influenced by temperature, we use separate parameters γ_C and d_C.

Considering the functional form of larval competition, temperature dependence in the development rates, and the assumption that only non-senescent adults contribute to reproduction, allows us to simplify the full model to

$$
\begin{aligned}
\frac{dL(t)}{dt} &= b_0 e^{\beta D(t)} A(t_1) S_E(t) - b_0 e^{\beta D(t)} A(t_3) S_L(t) - \left(d_L e^{\beta D(t)} + d_C e^{\gamma_C D(t)} L(t) + d_W e^{-\beta_W D(t)} \right) L(t) \\
\frac{dA(t)}{dt} &= b_0 e^{\beta D(t)} A(t_6) S_P(t) - b_0 e^{\beta D(t)} A(t_{10}) S_A(t) - \left(d_A e^{\beta D(t)} + d_W e^{-\beta_W D(t)} \right) A(t) \\
S_E(t) &= \exp\left(- \int_{t_1}^{t} \left(d_E e^{\beta D(\xi)} + d_W e^{-\beta_W D(\xi)} \right) d\xi \right) \\
S_L(t) &= \exp\left(- \int_{t_3}^{t_2} \left(d_E e^{\beta D(\xi)} + d_W e^{-\beta_W D(\xi)} \right) d\xi - \int_{t_2}^{t} \left(d_L e^{\beta D(\xi)} + d_C e^{\gamma_C D(\xi)} L(\xi) + d_W e^{-\beta_W D(\xi)} \right) d\xi \right) \\
S_P(t) &= \exp\left(- \int_{t_6}^{t_5} \left(d_E e^{\beta D(\xi)} + d_W e^{-\beta_W D(\xi)} \right) d\xi - \int_{t_5}^{t_4} \left(d_L e^{\beta D(\xi)} + d_C e^{\gamma_C D(\xi)} L(\xi) + d_W e^{-\beta_W D(\xi)} \right) d\xi \right. \\
&\qquad \left. - d_P \int_{t_4}^{t} e^{\beta D(\xi)} d\xi \right) \\
S_A(t) &= \exp\left(- \int_{t_{10}}^{t_9} \left(d_E e^{\beta D(\xi)} + d_W e^{-\beta_W D(\xi)} \right) d\xi - \int_{t_9}^{t_8} \left(d_L e^{\beta D(\xi)} + d_C e^{\gamma_C D(\xi)} L(\xi) + d_W e^{-\beta_W D(\xi)} \right) d\xi \right. \\
&\qquad \left. - d_P \int_{t_8}^{t_7} e^{\beta D(\xi)} d\xi - d_A \int_{t_7}^{t} e^{\beta D(\xi)} d\xi \right) \\
t_1 &= t - \tau_E(t) \\
t_2 &= t - \tau_L(t) \\
t_3 &= t_2 - \tau_E(t_2) \\
t_4 &= t - \tau_P(t) \\
t_5 &= t_4 - \tau_L(t_4) \\
t_6 &= t_5 - \tau_E(t_5) \\
t_7 &= t - \tau_A(t) \\
t_8 &= t_7 - \tau_P(t_7) \\
t_9 &= t_8 - \tau_L(t_8) \\
t_{10} &= t_9 - \tau_E(t_9)
\end{aligned}
$$

where the stage durations are given by

$$\frac{1}{\alpha_E} = \int_{t-\tau_E(t)}^{t} e^{\beta D(\xi)} d\xi$$
$$\frac{1}{\alpha_L} = \int_{t-\tau_L(t)}^{t} e^{\beta D(\xi)} d\xi$$
$$\frac{1}{\alpha_P} = \int_{t-\tau_P(t)}^{t} e^{\beta D(\xi)} d\xi$$
$$\frac{1}{\alpha_A} = \int_{t-\tau_A(t)}^{t} e^{\beta D(\xi)} d\xi$$

Note that the base temperature-dependent function belonging to the birth rate cancels out the denominator of the development rate function. The resulting model is a set of integro-delayed-differential equations with variable time delays.

Model transformation to development rate scale

The development rates for all stages share the same base temperature-dependent function, which means we can simplify the model further by doing an analytical transformation of integrations scales (*15*, *39*). In essence, rather than model the moth dynamics over time, we model them over a physiological scale that is related to development. The physiological scale is akin to a non-linear cumulative degree-day scale, but is more accurately the cumulative response of development to temperature rather than cumulative temperature. Let the new physiological scale (ϕ) be defined as

$$\phi(t) = \int_0^t e^{\beta D(\xi)} d\xi \tag{22}$$

by differentiating Eqn. 22 with respect to t and rearranging, we can write

$$\frac{d\tilde{t}}{d\phi} = \frac{1}{m(\phi)} \tag{23}$$
$$m(\phi) = e^{\beta D(t)} \tag{24}$$

where $\tilde{t}$ represents how time changes on the transformed scale. From the stage duration equations and Eq. 22, we can write

$$\phi(t - \tau_j(t)) = \int_0^{t-\tau_j(t)} e^{\beta D(\xi)} d\xi \tag{25}$$
$$= \int_0^t e^{\beta D(\xi)} d\xi - \int_{t-\tau_j(t)}^{t(t)} e^{\beta D(\xi)} d\xi \tag{26}$$
$$= \phi(t) - \frac{1}{\alpha_i} \tag{27}$$

which means that the variable delay equations on the time scale have become fixed delays on the transformed scale. The survivorship equations become

$$S_i(\phi) = \exp\left(-\int_{\phi-1}^{\phi} \frac{\delta_i(x)}{m(x)} dx\right) \tag{28}$$

which allows us to write the transformed model as

$$\frac{dL(\phi)}{d\phi} = b_0 A(\phi - \lambda_1) S_E(\phi) - b_0 A(\phi - \lambda_3) S_L(\phi) - \Omega_L(\phi) L(\phi) \tag{29}$$

$$\frac{dA(\phi)}{d\phi} = b_0 A(\phi - \lambda_6) S_P(\phi) - b_0 A(\phi - \lambda_{10}) S_A(t) - \Omega_A(\phi) A(\phi) \tag{30}$$

$$S_E(\phi) = \exp\left(-\int_{\phi-\lambda_1}^{\phi} \Omega_E(\xi) d\xi\right) \tag{31}$$

$$S_L(\phi) = \exp\left(-\int_{\phi-\lambda_3}^{\phi-\lambda_2} \Omega_E(\xi) d\xi - \int_{\phi-\lambda_2}^{\phi} \Omega_L(\xi) d\xi\right) \tag{32}$$

$$S_P(\phi) = \exp\left(-\int_{\phi-\lambda_6}^{\phi-\lambda_5} \Omega_E(\xi) d\xi - \int_{\phi-\lambda_5}^{\phi-\lambda_4} \Omega_L(\xi) d\xi - \int_{\phi-\lambda_4}^{\phi} \Omega_P(\xi) d\xi\right) \tag{33}$$

$$S_A(\phi) = \exp\left(-\int_{\phi-\lambda_{10}}^{\phi-\lambda_9} \Omega_E(\xi) d\xi - \int_{\phi-\lambda_9}^{\phi-\lambda_8} \Omega_L(\xi) d\xi - \int_{\phi-\lambda_8}^{\phi-\lambda_7} \Omega_P(\xi) d\xi - \int_{\phi-\lambda_7}^{\phi} \Omega_A(\xi) d\xi\right) \tag{34}$$

$$\Omega_E(x) = d_E + d_W e^{(-\beta_W - \beta) D(x)} \tag{35}$$

$$\Omega_L(x) = d_L + d_C e^{(\gamma_C - \beta) D(x)} L(x) + d_W e^{(-\beta_W - \beta) D(x)} \tag{36}$$

$$\Omega_P(x) = d_P + d_W e^{(-\beta_W - \beta) D(x)} \tag{37}$$

$$\Omega_A(x) = d_A + d_W e^{(-\beta_W - \beta) D(x)} \tag{38}$$

$$\lambda_1 = \frac{1}{\alpha_E} \tag{39}$$

$$\lambda_2 = \frac{1}{\alpha_L} \tag{40}$$

$$\lambda_3 = \frac{1}{\alpha_L} + \frac{1}{\alpha_E} \tag{41}$$

$$\lambda_4 = \frac{1}{\alpha_P} \tag{42}$$

$$\lambda_5 = \frac{1}{\alpha_P} + \frac{1}{\alpha_L} \tag{43}$$

$$\lambda_6 = \frac{1}{\alpha_P} + \frac{1}{\alpha_L} + \frac{1}{\alpha_E} \tag{44}$$

$$\lambda_7 = \frac{1}{\alpha_A} \tag{45}$$

$$\lambda_8 = \frac{1}{\alpha_A} + \frac{1}{\alpha_P} \tag{46}$$

$$\lambda_9 = \frac{1}{\alpha_A} + \frac{1}{\alpha_P} + \frac{1}{\alpha_L} \tag{47}$$

$$\lambda_{10} = \frac{1}{\alpha_A} + \frac{1}{\alpha_P} + \frac{1}{\alpha_L} + \frac{1}{\alpha_E} \tag{48}$$

The resulting model is a set of integro-delay-differential equations with fixed delays. Since most of the temperature-dependent rates cancel out (akin to non-dimensionalizing the model) casting the model on this scale also emphasizes where temperature impacts the model structure. Temperature comes into the model through the $D(\hat{t})$ function, and only impacts the mortality rates. In particular, the main influence is through the differential impact (i.e., relative to development) on larval competition and winter mortality. Interestingly, temperate is only expected to influence dynamics if a subset of the life-history rates responds differently to temperature than others. Figure S5 shows an example of the predicted dynamics when the model is driven with observed temperature from Kagoshima prefecture, and the corresponding physiological scale is shown in Fig. S6.

Stability analysis under constant temperature

Equilibrium analysis

Setting the derivative of the transformed model (Eqns. 29,30) to zero, yields the following expressions for larval ($\hat{L}$) and adult ($\hat{A}$) equilibrium at constant temperature T.

$$\hat{L} = \frac{\alpha_L \left(-\frac{\Omega_E}{\alpha_E} - \frac{\Omega_P}{\alpha_P} + \ln\left(\frac{b_0}{\Omega_A}\left(1 - \exp\left(-\frac{\Omega_A}{\alpha_A}\right)\right)\right)\right) - d_L - d_W e^{(-\beta_W - \beta)T}}{d_C e^{(\gamma_C - \beta)T}} \tag{49}$$

$$\hat{A} = \frac{\Omega_L \hat{L}}{b_0 \exp\left(-\frac{\Omega_E}{\alpha_E}\right)\left(1 - \exp\left(-\frac{\Omega_L}{\alpha_L}\right)\right)} \tag{50}$$

where the expressions for Ω_i are given by Eqs. 35-38. The equilibrium expressions are sufficiently complicated that it is difficult to gain insight from the analytical expressions. Fig. S7 shows an example of the change in larval and adult equilibrium abundance across temperature. The response shows a persistence boundary just below 10°C followed by a rapid increase in density and then a more gradual increase at higher temperatures.

Since $\hat{A}$ is strictly positive for positive $\hat{L}$, the persistence boundary is obtained from Eq. 49 by setting $\hat{L} = 0$. Again, since the expression is complicated, the boundary is solved numerically. We study the impact of each parameter on persistence across a wide range of parameter space (from 0.4 to 10 fold the estimated value) to evaluate system characteristics that are well beyond our point estimates for the two species that we have data on. Of all the parameters, the temperature exponent β and strength of winter mortality have the strongest impact on the persistence boundary (Fig. S8). Higher birth rates (b_o) cause a small decrease in the temperature of the persistence boundary and higher mortality scalars (d_i) causes a small increase. Both small and large development rates tend to increase the threshold temperature slightly. Since the temperature-dependent competition exponent γ_C drops out of the expression for persistence, it has no impact on the threshold. The parameters with the greatest influence are those associated with winter mortality (β_W and d_W) and the temperature exponent β. Specifically, increasing the rate at which the life-history rates increase with temperature (β) causes the system to persist at lower temperatures. Increasing the strength of winter mortality, either through higher dW or lower β_W, causes the system to be extinct at higher temperatures. To evaluate robustness of using a single temperature exponent for the warm-temperature mortality rate of all stages (g_i) and

a single temperature scalar for the winter mortality rate of all stages (g_W), we repeated the above analysis with stage-specific parameters. This did not have a qualitative impact on the results (Fig. S9).

To study the linear stability properties, we consider small deviations from the equilibrium of the form $x(\phi) = \hat{x} + \Delta_x(\phi)$ for each variable x. Introducing this into the transformed model (Eqns. 29, 30) and dropping higher order terms yields the following set of perturbation equations

$$\frac{d\Delta_L(\phi)}{d\phi} = b_0 \left(\hat{A}\Delta_{S_E}(\phi) + \hat{S}_E\Delta_A(\phi - \lambda_1) - \hat{A}\Delta_{S_L}(\phi) - \hat{S}_L\Delta_A(\phi - \lambda_3) \right) - \hat{L}\Delta_{\Omega_L}(\phi) - \hat{\Omega}_L\Delta_L(\phi) \quad (51)$$

$$\frac{d\Delta_A(\phi)}{d\phi} = b_0 \left(\hat{A}\Delta_{S_P}(\phi) + \hat{S}_P\Delta_A(\phi - \lambda_6) - \hat{A}\Delta_{S_A}(\phi) - \hat{S}_A\Delta_A(\phi - \lambda_{10}) \right) - \hat{\Omega}_A\Delta_A(\phi) \quad (52)$$

Survivorship and mortality perturbations can be further simplified. The tricky parts are the survivorship perturbations that require integrating over larval dynamics. Substituting the deviation expression into the survivorship equations with larval density dependence lets us write

$$\Delta_{S_i}(\phi) = \hat{S}_i \left(\exp\left(-d_C e^{(\gamma_C - \beta)T} \int_a^b \Delta_L(x)dx \right) - 1 \right) \quad (53)$$

where a and b are the start and end time-points for a particular stage. Using the series expansion for an exponential and dropping all terms with orders of $\Delta_L(\phi)$ greater than one, we arrive at

$$\Delta_{S_i}(\phi) = -\hat{S}_i d_C e^{(\gamma_C - \beta)T} \int_a^b \Delta_L(x)dx \quad (54)$$

Using the above relationships, the survivorship and mortality perturbations become

$$\Delta_{\Omega_L}(\phi) = d_C e^{(\gamma_C - \beta)T} \Delta_L(\phi) \quad (55)$$

$$\Delta_{S_E}(\phi) = 0 \quad (56)$$

$$\Delta_{S_L}(\phi) = -\hat{S}_L d_C e^{(\gamma_C - \beta)T} \int_{\phi - \lambda_2}^{\phi} \Delta_L(x)dx \quad (57)$$

$$\Delta_{S_P}(\phi) = -\hat{S}_P d_C e^{(\gamma_C - \beta)T} \int_{\phi - \lambda_5}^{\phi - \lambda_4} \Delta_L(x)dx \quad (58)$$

$$\Delta_{S_A}(\phi) = -\hat{S}_A d_C e^{(\gamma_C - \beta)T} \int_{\phi - \lambda_9}^{\phi - \lambda_8} \Delta_L(x)dx \quad (59)$$

Substituting these into the perturbation Eqns. 51-52 yields

$$\frac{d\Delta_L(\phi)}{d\phi} = b_0\hat{S}_E\Delta_A(\phi-\lambda_1) - b_0\hat{S}_L\Delta_A(\phi-\lambda_3) + b_0\hat{A}\hat{S}_L d_C e^{(\gamma_C-\beta)T}\int_{\phi-\lambda_2}^{\phi}\Delta_L(x)dx - \left(\hat{L}d_C e^{(\gamma_C-\beta)T} + \hat{\Omega}_L\right)\Delta_L(\phi) \quad (60)$$

$$\frac{d\Delta_A(\phi)}{d\phi} = b_0\hat{S}_P\Delta_A(\phi-\lambda_6) - b_0\hat{S}_A\Delta_A(\phi-\lambda_{10}) - \hat{\Omega}_A\Delta_A(\phi) + b_0\hat{A}d_C e^{(\gamma_C-\beta)T}\left(\hat{S}_A\int_{\phi-\lambda_9}^{\phi-\lambda_8}\Delta_L(x)dx - \hat{S}_P\int_{\phi-\lambda_5}^{\phi-\lambda_4}\Delta_L(x)dx\right) \quad (61)$$

Using an exponential trial solution of the form $\Delta_i(\phi) = \Delta_i(0)\exp(r\phi)$ where $\Delta_i(0)$ is the initial perturbation, we can write the dynamics of the perturbation over ϕ as the following set of algebraic equations

$$0 = \left(d_C e^{(\gamma_C-\beta)T}\left(\frac{b_0\hat{A}\hat{S}_L}{r}\left(1-e^{-r\lambda_2}\right) - \hat{L}\right) - \hat{\Omega}_L - r\right)\Delta_L(0) + b_0\left(\hat{S}_E e^{-r\lambda_1} - \hat{S}_L e^{-r\lambda_3}\right)\Delta_A(0) \quad (62)$$

$$0 = b_0\hat{A}d_C e^{(\gamma_C-\beta)T}\left(\frac{\hat{S}_A}{r}\left(e^{-r\lambda_8} - e^{-r\lambda_9}\right) - \frac{\hat{S}_P}{r}\left(e^{-r\lambda_4} - e^{-r\lambda_5}\right)\right)\Delta_L(0) + \left(b_0\hat{S}_P e^{-r\lambda_6} - b_0\hat{S}_A e^{-r\lambda_{10}} - \hat{\Omega}_A - r\right)\Delta_A(0) \quad (63)$$

where

$$\hat{S}_E = \exp\left(-\frac{d_E + d_W e^{(-\beta_W-\beta)T}}{\alpha_E}\right) \quad (64)$$

$$\hat{S}_L = \hat{S}_E\exp\left(-\frac{d_L + d_C e^{(\gamma_C-\beta)T}\hat{L} + d_W e^{(-\beta_W-\beta)T}}{\alpha_L}\right) \quad (65)$$

$$\hat{S}_P = \hat{S}_L\exp\left(-\frac{d_P + d_W e^{(-\beta_W-\beta)T}}{\alpha_P}\right) \quad (66)$$

$$\hat{S}_A = \hat{S}_P\exp\left(-\frac{d_A + d_W e^{(-\beta_W-\beta)T}}{\alpha_A}\right) \quad (67)$$

$$\hat{\Omega_L} = d_L + d_C e^{(\gamma_C-\beta)T}\hat{L} + d_W e^{(-\beta_W-\beta)T} \quad (68)$$

$$\hat{\Omega_A} = d_A + d_W e^{(-\beta_W-\beta)T} \quad (69)$$

The transcendental nature of the equations are caused by the delays in the system and must be studied numerically. Fig. S10 shows some of the leading eigenvalues at different temperatures. Starting at low temperatures where no positive density of moths is predicted (Fig. S7), the system transitions from unstable to stable near 10°C for the parameter set in Table S2, which corresponds to the persistence boundary. The transition is via a single real eigenvalue crossing the zero line, which is a *stationary bifurcation*. As temperature increases, the density of moths increases and the system remains stable until near 13°C where a pair of complex conjugates cross the zero real axis indicating a *Hopf bifurcation*. As with the persistence boundary, the Hopf bifurcation is qualitatively robust to the details of temperature scaling. For example, allowing for stage-specific differences in the temperature scaling still yields a critical bifurcation at around 15°C.

Bifurcations

To solve for the leading eigenvalue, we do a root minimization of Eqns. 62-63 in the vicinity of the leading eigenvalue. The challenge is to find an approximation to the *leading* eigenvalue out of the infinite number of possible solutions to the delayed-differential equations, such that the root minimization identifies the correct solution (i.e., does not lead to one of the subdominant roots). To do this, we develop an equivalent Linear Multistep (LMS) transition matrix of the perturbation equations (*40*). The leading eigenvalue of this matrix is then an approximation of the leading eigenvalue of the full perturbation equations. To start, we use the following form of the perturbation equations that are easier to work with

$$\frac{d\Delta_L(\phi)}{d\phi} = a_1\Delta_A(\phi_1) - a_2\Delta_A(\phi_3) - a_4\Delta_L(\phi) + a_3\int_{\phi_2}^{\phi}\Delta_L(x)dx$$
$$\frac{d\Delta_A(\phi)}{d\phi} = a_5\Delta_A(\phi_6) - a_6\Delta_A(\phi_9) - a_7\Delta_A(\phi) + a_8\int_{\phi_8}^{\phi_7}\Delta_L(x)dx - a_9\int_{\phi_5}^{\phi_4}\Delta_L(x)dx$$
$$a_1 = b_0\hat{S}_E$$
$$a_2 = b_0\hat{S}_L$$
$$a_3 = b_0\hat{A}\hat{S}_L d_{L2} e^{(\gamma_C-\beta)T}$$
$$a_4 = \left(\hat{L}d_{L2}e^{(\gamma_C-\beta)T} + \hat{\Omega}_L\right)$$
$$a_5 = b_0\hat{S}_P$$
$$a_6 = b_0\hat{S}_A$$
$$a_7 = \hat{\Omega}_A$$
$$a_8 = b_0\hat{A}d_{L2}e^{(\gamma_C-\beta)T}\hat{S}_A$$
$$a_9 = b_0\hat{A}d_{L2}e^{(\gamma_C-\beta)T}\hat{S}_P$$
$$\phi_1 = \phi - \lambda_1$$
$$\phi_2 = \phi - \lambda_2$$
$$\phi_3 = \phi - \lambda_3$$
$$\phi_4 = \phi - \lambda_4$$
$$\phi_5 = \phi - \lambda_5$$
$$\phi_6 = \phi - \lambda_6$$
$$\phi_7 = \phi - \lambda_8$$
$$\phi_8 = \phi - \lambda_9$$
$$\phi_9 = \phi - \lambda_{10}$$

Following Engelboroughs & Roose (*40*), we create the $2n$ x $2n$ matrix that describes the Linear Multistep. The time-span goes from current time (ϕ) to the historical time that just includes the longest delay (ϕ_9) plus any extra locations required for reliable interpolation of delays using Lagange polynomials near the edges. The number of grid locations over the time interval is given by n. The first n rows of the matrix are the larval stages, and the last n rows are the adult stages. All matrix elements are zero except for the following transitions

- Time shift for larvae and adults ($i \in \{1, 2, .., n-1\}$)

$$M[i+1,i] = 1$$
$$M[n+i+1,n+i] = 1$$

- Derivative contribution to larvae from non-lagged terms ($i \in \{1,2,..,k\}$)

$$M[1,i] = M[1,i] - \eta[i+1]/(\eta[1] + ha_4)$$

- Derivative contribution to larvae from ϕ_1 lagged term ($l \in o_{\phi_1}$)

$$M[1,n+l] = M[1,n+l] + \frac{a_1 h}{\eta[1] + ha_4} \prod_{q \in o_{\phi_1}; q \neq l} \frac{\phi_1 - X_q}{X_l - X_q}$$

- Derivative contribution to larvae from ϕ_3 lagged term ($l \in o_{\phi_3}$)

$$M[1,n+l] = M[1,n+l] - \frac{a_2 h}{\eta[1] + ha_4} \prod_{q \in o_{\phi_3}; q \neq l} \frac{\phi_3 - X_q}{X_l - X_q}$$

- Derivative contribution to larvae from the integral term ($l \in o_{\phi_p}$; $\phi_p \in \{\phi, \phi + \hat{h}, \ldots, \phi_2\}$)

$$M[1,n+l] = M[1,n+l] + \hat{h} \sum_{\phi_p = \phi}^{\phi_2} \left(\frac{a_3 h}{\eta[1] + ha_4} \prod_{q \in o_{\phi_p}; q \neq l} \frac{\phi_p - X_q}{X_l - X_q} \right)$$

- Derivative contribution to adults from non-lagged terms ($i \in \{1,2,..,k\}$)

$$M[n+1,n+i] = M[n+1,n+i] - \eta[i+1]/(\eta[1] + ha_7)$$

- Derivative contribution to adults from ϕ_6 lagged term ($l \in o_{\phi_6}$)

$$M[n+1,n+l] = M[n+1,n+l] + \frac{a_5 h}{\eta[1] + ha_7} \prod_{q \in o_{\phi_6}; q \neq l} \frac{\phi_6 - X_q}{X_l - X_q}$$

- Derivative contribution to adults from ϕ_9 lagged term ($l \in o_{\phi_9}$)

$$M[n+1,n+l] = M[n+1,n+l] - \frac{a_6 h}{\eta[1] + ha_7} \prod_{q \in o_{\phi_9}; q \neq l} \frac{\phi_9 - X_q}{X_l - X_q}$$

- Derivative contribution to adults from the first integral term ($l \in o_{\phi_p}$; $\phi_p \in \{\phi_7, \phi_7 + \hat{h}, \ldots, \phi_8\}$)

$$M[n+1,l] = M[n+1,l] + \hat{h} \sum_{\phi_p = \phi_7}^{\phi_8} \left(\frac{a_8 h}{\eta[1] + ha_7} \prod_{q \in o_{\phi_p}; q \neq l} \frac{\phi_p - X_q}{X_l - X_q} \right)$$

- Derivative contribution to adults from the second integral term ($l \in o_{\phi_p}$; $\phi_p \in \{\phi_4, \phi_4 + \hat{h}, \ldots, \phi_5\}$)

$$M[n+1,l] = M[n+1,l] - \hat{h} \sum_{\phi_p = \phi_4}^{\phi_5} \left(\frac{a_9 h}{\eta[1] + ha_7} \prod_{q \in o_{\phi_p}; q \neq l} \frac{\phi_p - X_q}{X_l - X_q} \right)$$

where $h = (\phi_9 - \phi)/n$ is the step size, $k = 6$ is the order of the *Backwards Differentiation Formula*, and $\eta = \{147/60, -6, 15/2, -20/3, 15/4, -6/5, 1/6\}$ is the accompanying set of coefficients for the LMS scheme. Grid locations X are spread over a fine step from current time (on the phi scale) to the

maximum delay in the system, and o_{ϕ_p} is a vector of locations in X that spread 3 steps on either side of a particular lag ϕ_p. Integrals are calculated by further discritizing the time intervals with step size $\hat{h} = 0.1h$ and summing the resulting interpolated lagged values.

Stability and bifurcation results

The real and imaginary components of the leading eigenvalue indicate both the stability of the system and aspects of the transient dynamics. Figures S11, S12 illustrate this for different combinations of β_W and temperature. Starting at cool temperatures, there is no positive moth density when the temperature is below the persistence boundary. Once temperature is warm enough for persistence, the equilibrium is stable (Fig. S11) with a pair of non-zero complex conjugates (Fig. S12), which means that the transient dynamics would decay with oscillations to the equilibrium. Once across the Hopf line, the eigenvalues are pairs of non-zero complex conjugates with positive real parts that indicate sustained limit cycles. The magnitude of the complex component is relatively constant once over the Hopf line, indicating that the frequency is not sensitive to differences in parameter values within the unstable regions.

Tracing the Hopf line for each parameter across different temperatures allows us to evaluate the influence that each has on the critical temperature that determines system stability. Using the same approach as for the persistence boundary, we find that some parameters have a greater influence on the critical temperature than others (Fig. S13). Increasing the temperature exponent (β) has a relatively large effect causing the system to become unstable at cooler temperatures. Increasing the birth rate (b_o) and many of the development rates (α_i) causes the system to cycle at lower temperatures, but they do not have as strong an effect as the temperature exponent. Adult senescence rate and temperature exponent have the opposite effect on stability (dotted lines Fig. S13). When the adult development is too fast, the system becomes more stable with respect to temperature likely because it reduces the total birth rate. When adult development is too slow, the system also becomes more stable because it reduces the destabilizing effect of a short adult reproductive period. Increasing the mortality scalars (d_i and d_{W_i}) have the effect of stabilizing the system, whereas decreasing the strength of winter mortality (by increasing β_W) has a strong destabilizing effect on the system.

Stability analysis under seasonally driven temperature

The behaviour of the driven system is different than the asymptotic dynamics because transient dynamics are chasing an ever moving attractor. To characterize dynamics under driven seasonal changes, we consider both a step change in temperature, and seasonally driven changes in temperature. With an abrupt change in temperature from 10°C to 25°C, which roughly reflects the March to July transition in Japan, the system begins cycling immediately and the amplitude increases rapidly over the first 2 cycles (Fig. S14). With an abrupt change in temperature from 25°C to 9°C, which roughly represents the September to December transition in Japan, the system stops cycling immediately with strongly damped oscillations (Fig. S15). Note that the period of the transient dynamics is 2-3 times the period of the generation cycles, which means that transient dynamics will not confound our analysis of the generation cycles using wavelets.

If we consider seasonally-driven changes in temperature, the model predicts that the asymptotic dy-

namics will most often be either in the cycling state or in the strongly damped stable state heading to extinction (Fig. 2). Figure S16 shows the transient moth dynamics when the model is driven with observed seasonal temperature data from Kagoshima. The predicted transient dynamics follow the qualitative aspects of the asymptotic dynamics fairly well. The population cycles during the period of instability (blue lines), and rapidly tend toward the persistence boundary during cold periods. There is a lag in moth density at the onset of spring owing to low winter densities. The lag appears long enough to have the transient dynamics miss a full cycle. The period of time where the asymptotic dynamics predict a stable equilibrium (gray lines) is small relative to when cyclic or extinction dynamics are expected, which means the system is best to be thought of as flipping between no persistence and limit cycles as the season progresses. The transient dynamics are responsible for the threshold in amplitude appearing at a higher temperature than the Hopf bifurcation. Figure S17 shows a few example years of the predicted larval and adult dynamics superimposed with the temperature driver. While the transient dynamics are expected to roughly follow the asymptotic dynamics, there are some differences. To account for this difference, we develop the predictions from the wavelet and threshold analysis (see the sections on *Wavelet decomposition* and *Threshold analysis*) using the model driven with observed seasonal temperature in Japan.

Wavelet decomposition

Moth dynamics (Fig. 1) are sampled on average every 5 days, but not necessarily evenly. Since the wavelet decomposition methods require evenly spaced data, we convert the dataset to a grid with regular 5 day intervals using linear interpolation. The class of pesticide used to control the moth has changed over the past half century (Fig. 1), but since there is no correlation between their use and the population dynamics of the moth we analyze the time series as one large dataset rather than in sections. We applied a Morlet wavelet to the measured moth densities—now evenly spaced through time—using the *cwt()* function in the *Rwave* R library (*18*). All analyses were done in the R statistical framework (*41*). Wavelet decomposition of the raw time-series is shown in Fig. S18. Our primary interest is to compare the annual and sub annual components of the moth dynamics with temperature. This can be done by reconstructing the time-series over the specific frequency range (*42*). To ensure quality reconstruction, we fit a wavelet to the data using a wide range in wavelet period (15 octaves) and a high resolution within each octave (256 voices). The close agreement between the full reconstructed time-series (i.e., using all frequencies) with the raw data (Fig. S19) indicates that the numbers of octaves and voices are sufficient.

The global power spectrum indicates two dominant peaks at periods of $\tau = 365$ days and $\tau = 45$ days, which correspond to the annual and sub-annual cycles respectively (Fig. S20). To reconstruct each type of cycle, we create a window that is 35% of the peak value on each side, which captures the main dynamics around that focal frequency (Fig. S18). Moth dynamics at each focal frequency are shown in Fig. 3.

The corresponding wavelet and global spectrum are shown in Figs. S21, S22 for simulated moth dynamics using the parameterized model (see *Model development and parameterization*) driven with the observed temperatures in Japan. Many key characteristics of the observed moth dynamics are well captured well by a lab-based understanding of how life-history traits respond to temperature. The predicted dynamics capture the annual cycle, the faster generation cycles, and the fact that the generation

cycles turn on and off over a season (Fig. S23). The predicted period of the sub-annual cycles is slightly longer than the observed (*15*), and we characterize the predicted cycles relative to this dominant period of τ=55 days. The reconstructed annual and sub-annual cycles from the simulated dynamics (Fig. S23) are used to generate the predicted transient dynamics in the threshold analysis below.

Wavelets can also be used to calculate the proportion variation explained by our model. Specifically, we scale each wavelet so that the total amount of spectral power in the observed and simulated wavelets is the same. Taking the absolute value of the difference between the scaled wavelets provides the amount of unexplained spectral power, and dividing this by the expected difference from comparing random frequency and time points gives the proportion variance unexplained. Converting this to proportion explained, we find that our model explains 50% of the special power in the half century of observed moth dynamics. The model captures the dominant annual and sub-annual frequencies, and the seasonal change in the sub-annual cycles very well. But it does not predict the year-to-year variation in peak densities, which is an interesting avenue for future study.

Threshold analysis

The model given by Eqns. 29, 30 predicts that moth populations should transition from stable dynamics at cooler temperatures to cyclic dynamics at warmer temperatures (Fig. 2). The transition is predicted to occur via a Hopf bifurcation around 13°C. To test this prediction, we used the temporal dynamics in moth density over the last 40 years (1971-2011) where we have high-quality temperature data from the trap site (temperature during the first 10 years was measured at a different frequency). The sub-annual amplitude was generated from the wavelet reconstruction (see *Wavelet decomposition*) at the same frequency as the observations of moth density (every 5 days). To evaluate the change in amplitude over the season, we first divide the sub-annual amplitude time-series into annual sections at January 1st of each year, and then split each year into *spring* and *fall* phases based on the peak amplitude of the sub-annual cycles because we have reason to expect that the transient dynamics may be different when the Hopf point is crossed from below versus above (see *Stability analysis under seasonally driven temperature*). The result is 40 spring and 40 fall transitions, which we analyze to estimate the threshold temperature and how amplitude depends on temperature.

We use the following piecewise linear regression

$$y = \begin{cases} a + bx & \text{if } x < x_c \\ a + (b-d)x_c + dx & \text{otherwise} \end{cases} \tag{70}$$

where y is the sub-annual cycle amplitude from the wavelet reconstruction obtained from the raw data, x is the observed mean temperature on that day, x_c is the threshold temperature to be estimated from the data, and a, b, c are parameters fit to each year. We fit the piecewise linear regression to the spring and fall amplitudes using a non-linear mixed-effects model. Year is treated as a random effect and the amplitude within a year is assumed to be serially dependent according to a first order moving average process. Fits were done using the *nlme()* library (*43*) in the R statistical framework and the threshold is estimated using profile likelihood (*41*). There is strong statistical support for the presence of a threshold in both the spring (likelihood ratio test: $\chi^2_4 = 689.6$, p<0.0001) and fall (likelihood ratio test:

$\chi^2_4 = 1338.8$, $p<0.0001$) phases, and for the presence of an autocorrelation model (spring: ΔAIC=236, fall: ΔAIC=1210). Maximum likelihood estimate of the threshold is 15.0°C (95% CI's: {14.4,15.5}) for the spring transition and 19.7°C (95% CI's: {19.3-20.1}) for the fall transition (Fig. S24). These results are robust to the assumption of a single threshold across years. Fitting a separate threshold to each year yields an estimated threshold of 14.4°C (95% CI's: {13.4-15.3}) and 16.7°C (95% CI's: {14.5-19.0}) for spring and fall respectively.

The predicted change in stability under constant temperature gives an indication of where the threshold may occur, but dynamics under seasonally variable temperature are expected to show some influence of transient dynamics (see *Stability analysis under seasonally driven temperature*). We therefore estimate the threshold from simulated data using the historical temperatures at the tea field site in Japan. The estimated threshold for spring and fall phases are 18.8°C (95% CI's: {16.8-20.7}) and 18.6°C (95% CI's: {16.7-20.4}) respectively (Fig. 4). These thresholds compare well with the empirical data.

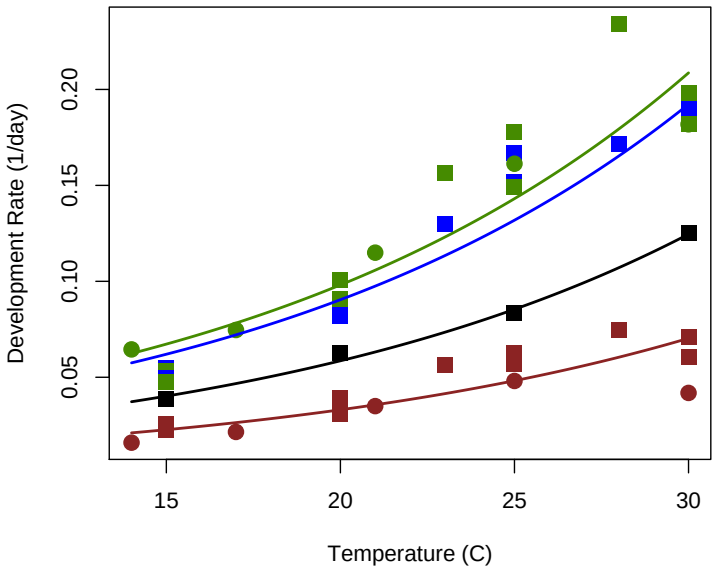

Fig. S1. Stage development rates for two species. Data for *A. honmai* (squares) is from Nabeta *et al.* 2005 (*32*) and Kodomari *et al.* 2003 (*33*), and data for *A. orana* (circles) is from Milonas 2000 (*25*). Solid lines are fits for the function $h_i = \alpha_i e^{\beta D}$, where α_i is different for each stage i, but all stages and life history traits share the same β. Colours denote different stages (eggs: blue, larvae: red, pupae: green, adult: black).

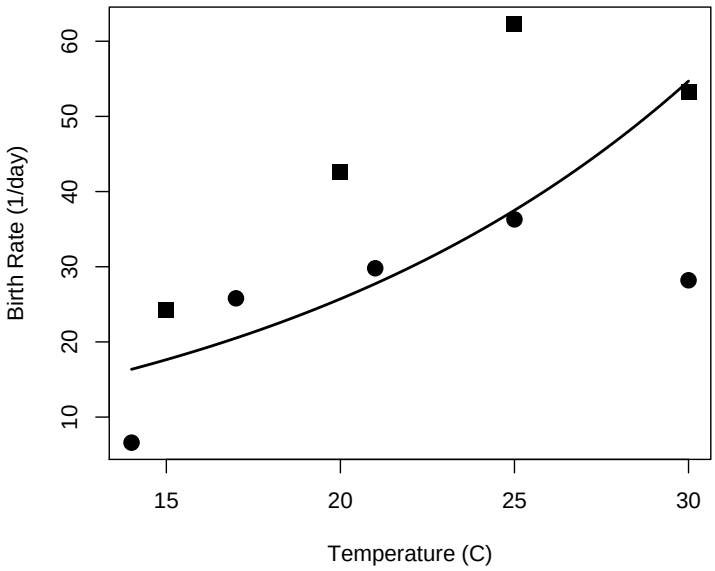

Fig. S2. Per-capita birth rates from laboratory experiments. Data sources are the same as in Fig. S1. Solid lines are fits for the function $b = b_o e^{\beta D}$.

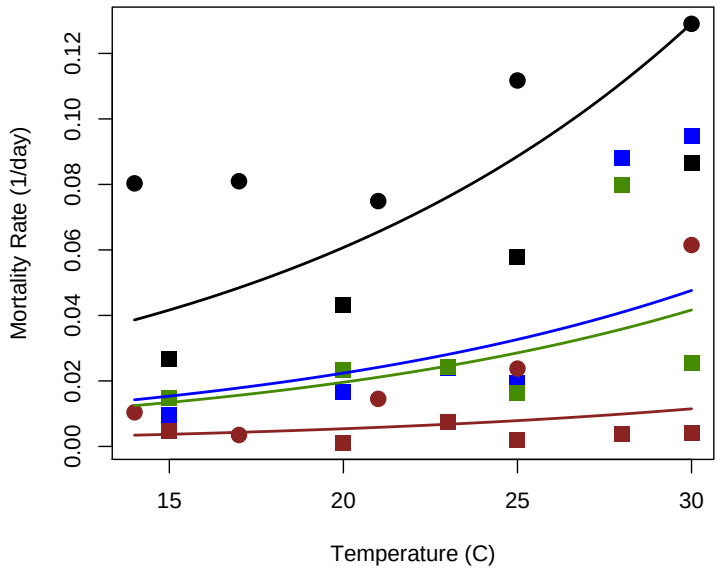

Fig. S3. Per-capita mortality rates from laboratory data. Data sources are the same as in Fig. S1. Solid lines are fits for the function $g_i = d_i e^{\beta D}$, where d_i are different for each stage i, but all stages and all life history traits share the same β.

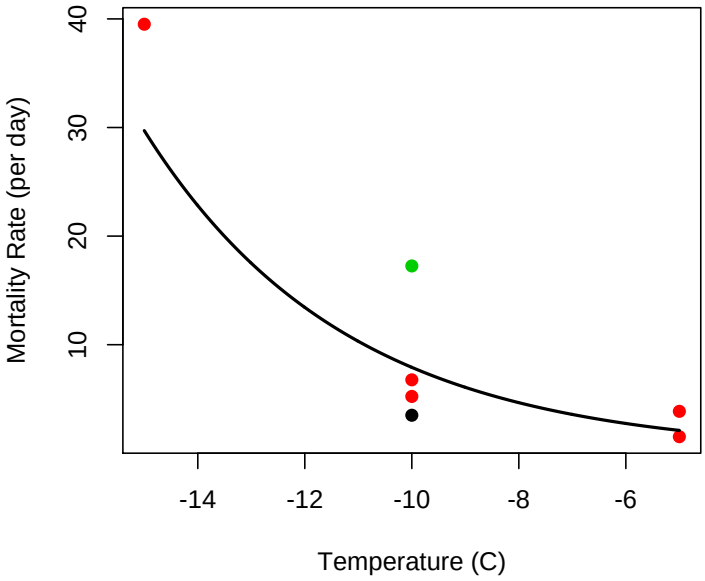

Fig. S4. Per-capita mortality rates for winter temperatures from laboratory data on *A. orana* from Jo & Kim (*38*). Colours are as in Fig. S1. Solid line shows the fit of the function $g_W = d_W e^{-\beta_W D}$, where d_W is the larval winter mortality scalar and β_W is the winter mortality exponent.

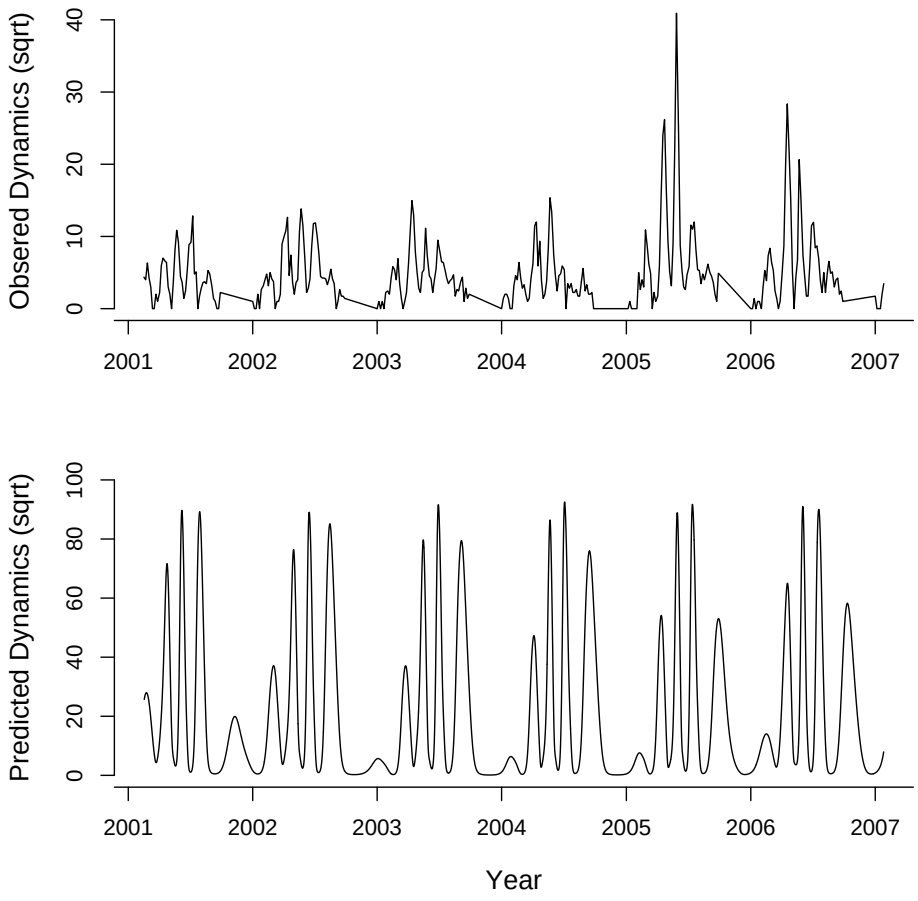

Fig. S5. Snapshot of the observed (top panel) and predicted (bottom panel) moth dynamics. Observed dynamics are a snapshot of the full time-series (Fig. 1). Predicted dynamics are for the parameter estimates in Table S2 with $\gamma_C = 4\,\mathrm{e}\,{-2}$ and $d_C = 1\,\mathrm{e}\,{-6}$.

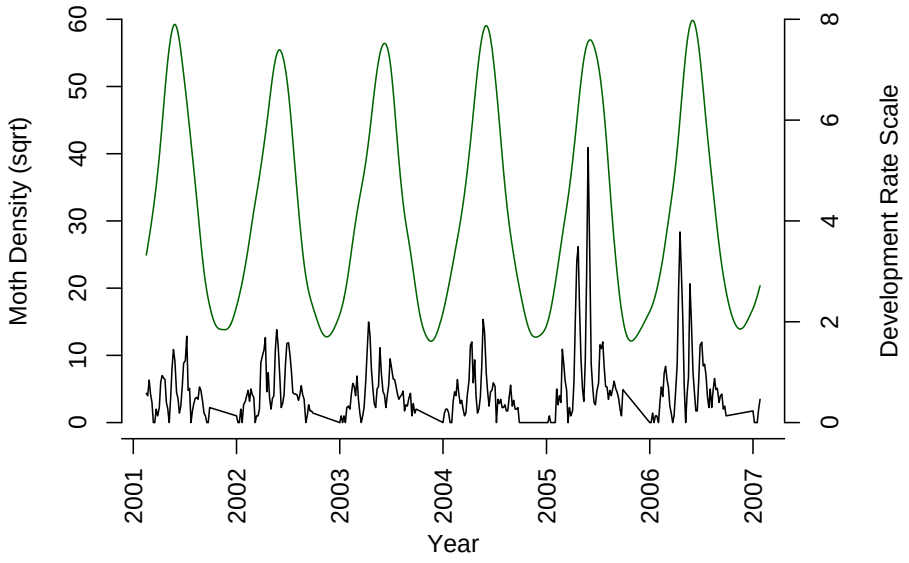

Fig. S6. Observed moth dynamics (black line) and the physiological scale (Eqn. 24) derived from the observed temperature dynamics.

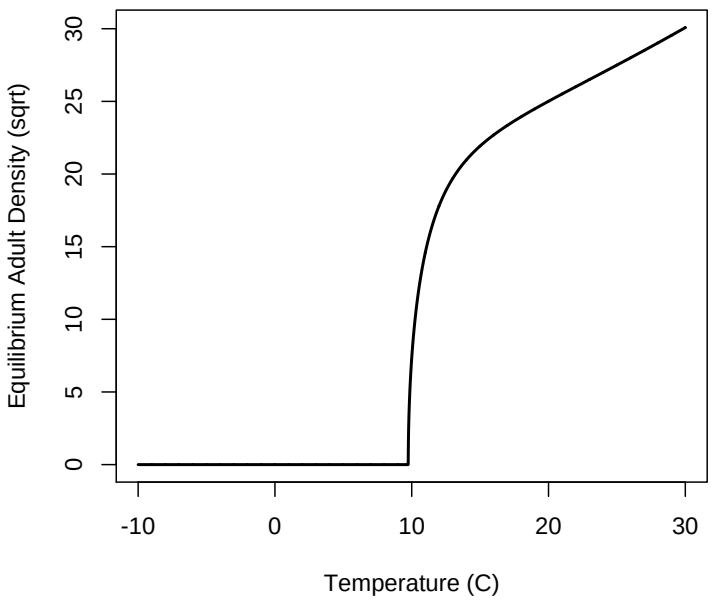

Fig. S7. Example predicted equilibrium response of adult density to temperature. Persistence boundary is just below 10°C (negative densities are set at zero). Predicted equilibria are for the parameter estimates in Table S2 with $\gamma_C = 4\,\mathrm{e}\,{-2}$ and $d_C = 1\,\mathrm{e}\,{-6}$.

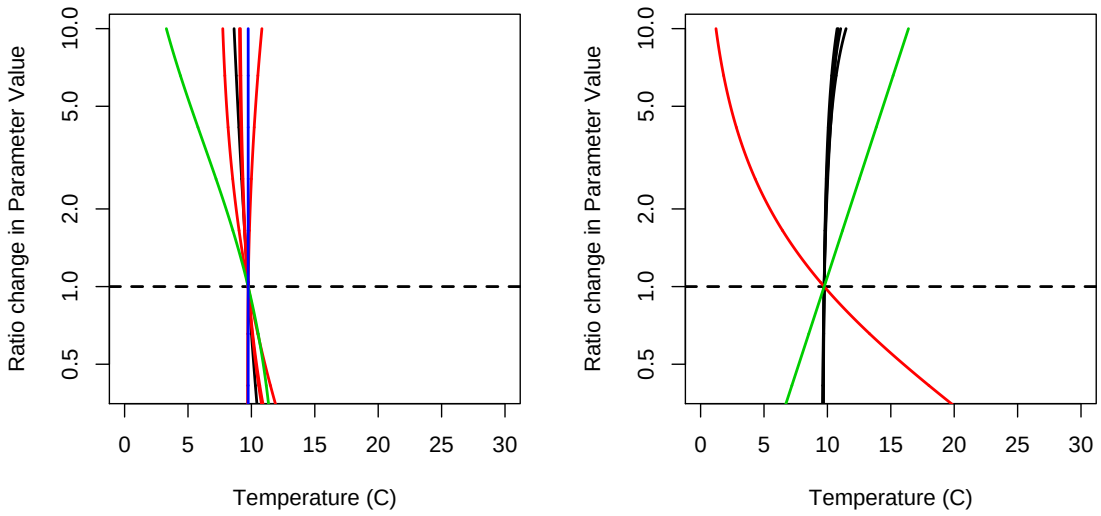

Fig. S8. Temperature of the persistence boundary (i.e., temperature when equilibrium larval density is zero) as a function of different parameter values. The y-axis is change in parameter estimate relative to the estimated value (horizontal dashed line). Left panel shows the birth rate (b_o; black line), development rates (α_i; red lines), temperature dependence in competition (γ_C; blue line) and temperature exponent for life history traits (β; green line). Right panel shows mortality scalars (d_i; black lines), winter mortality scalar (d_W; green line) and winter mortality exponent (β_W; red line). Parameter estimates are given in Table S2 with $\gamma_C = 4\,\mathrm{e}-2$ and $d_C = 1\,\mathrm{e}-6$.

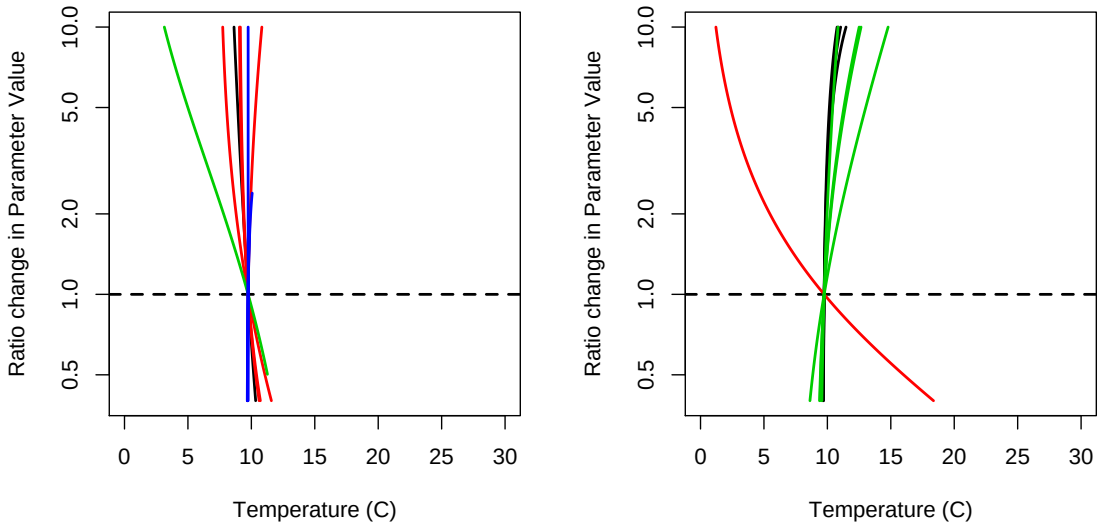

Fig. S9. Temperature of the persistence boundary expanded to include stage-specific parameters for warm temperature mortality exponents (β_i) and for winter mortality scalars (d_{Wi}). Colours and panels correspond to Fig S8.

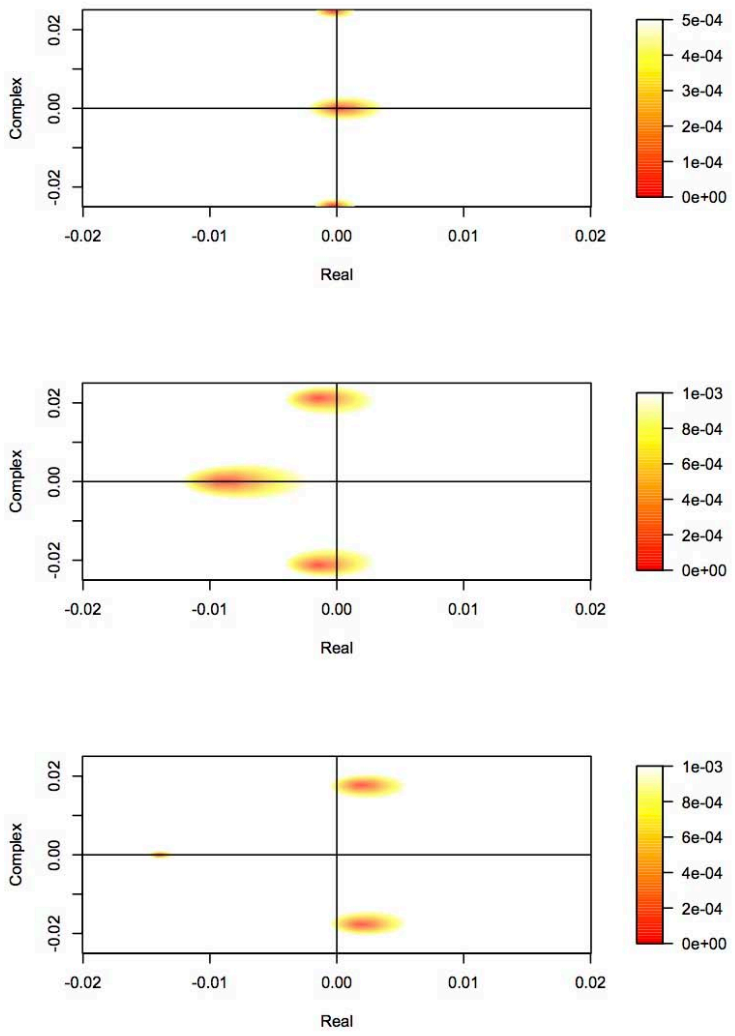

Fig. S10. Eigenvalues of the perturbation Eqns. 62-63 at three temperatures: 9.7°C (top panel), 11°C (middle panel) and 20°C (bottom panel). The heat map shows the absolute value of the LHS of Eqns. 62-63. The roots are found in the middle of the red area. The two leading eigenvalues are shown, and all remaining eigenvalues occur beyond the scale shown. Parameter values used are those given in Table S2 with $\gamma_C = 4\,\mathrm{e}-2$ and $d_C = 1\,\mathrm{e}-6$. The corresponding equilibrium densities are shown in Fig. S7.

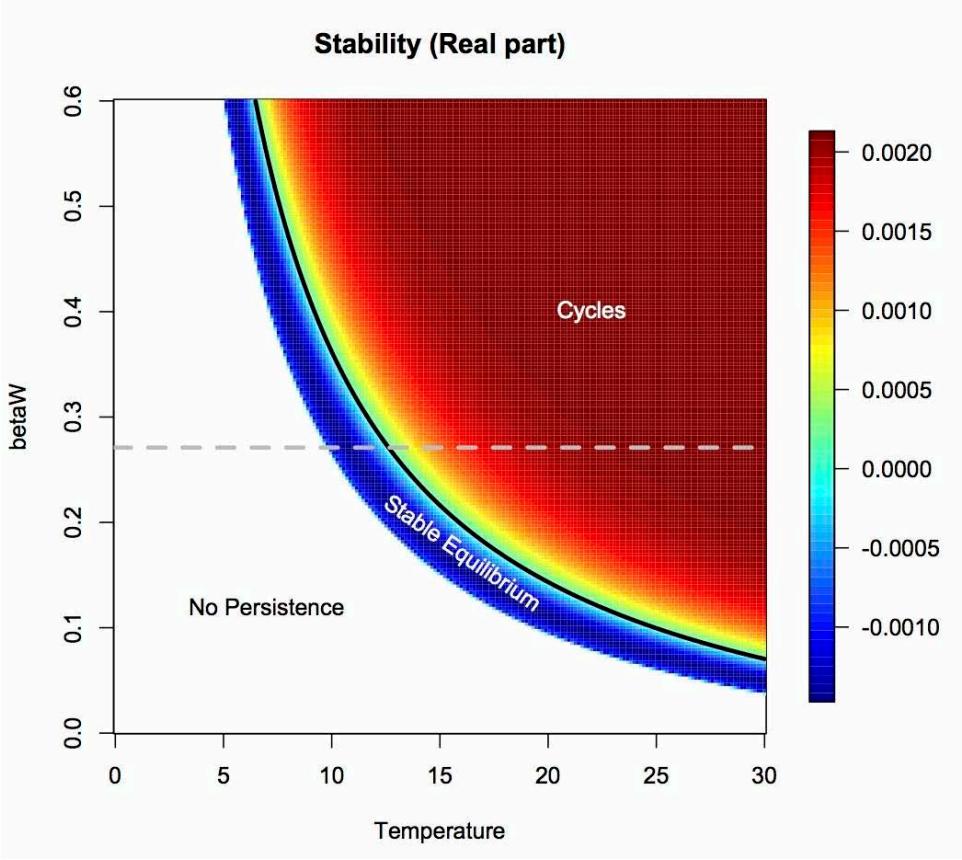

Fig. S11. Real component of the leading eigenvalue as a function of temperature and β_W. Regions with colour delineate areas where the equilibrium has a positive equilibrium (i.e., persistence), and the heat map gives the magnitude of the real part. The horizontal dashed line is the estimated parameter value and the solid black line delineates the Hopf line.

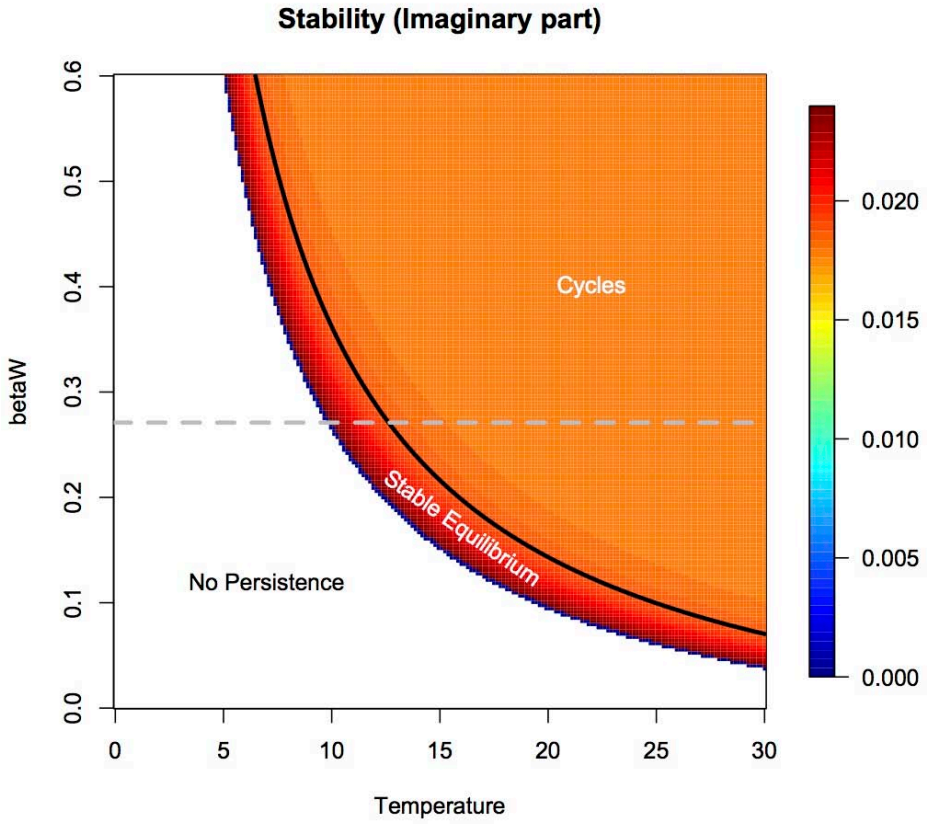

Fig. S12. Complex component of the leading eigenvalue as a function of temperature and β_W. Regions with colour delineate areas where the equilibrium has a positive equilibrium, and the heat map denotes the absolute value of the imaginary part. The horizontal dashed line is the estimated parameter value and the solid black line delineates the Hopf line.

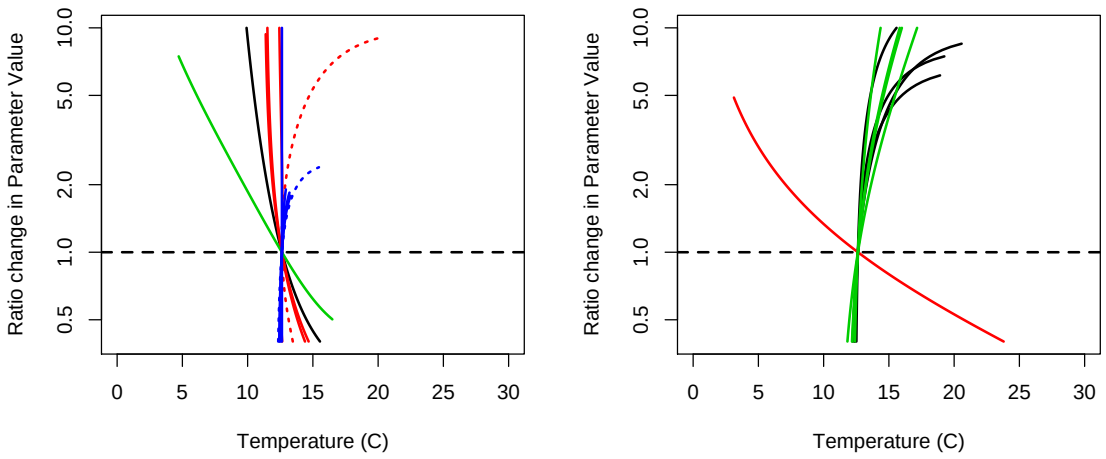

Fig. S13. Temperature of the Hopf line (i.e., temperature when system changes stability) as a function of different parameter values. The y-axis is change in parameter estimate relative to the estimated value (horizontal dashed line). Left panel shows the birth rate (b_o; black line), development rates (α_i; red lines with adult stage shown as a dotted line), temperature dependence in competition (γ_C) and stage-specific warm temperature exponent (blue line with adult stage shown as a dotted line) and temperature exponent for the remaining life history traits (β; green line). Right panel shows mortality scalars (d_i; black lines), winter mortality scalars (d_{W_i}; green line) and winter mortality exponent (β_W; red line). Parameter estimates are given in Table S2 with $\gamma_C = 4\,\mathrm{e}\,{-2}$ and $d_C = 1\,\mathrm{e}\,{-6}$.

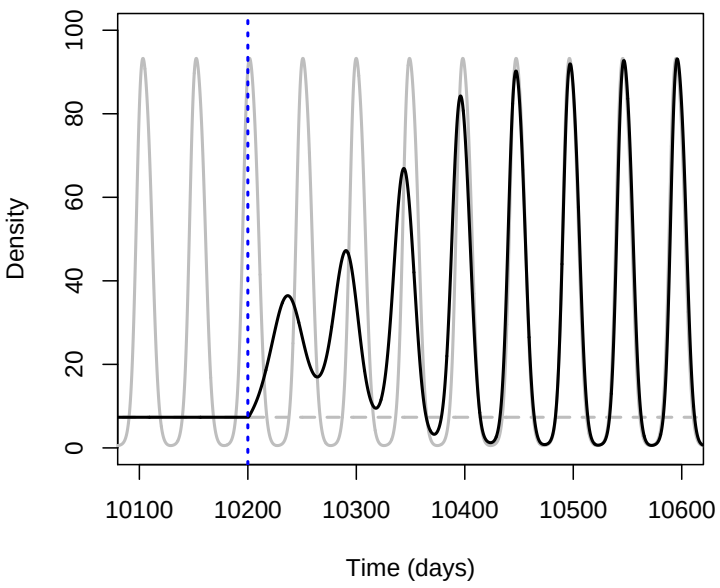

Fig. S14. Asymptotic moth dynamics predicted at 10°C (dashed tray line) and at 25°C (solid tray line). Transient dynamics (black line) are shown starting at the asymptotic dynamics of 10°C, with an abrupt change to 25°C at the blue line. Parameter estimates are given in Table S2 with $\gamma_C = 4\,\mathrm{e}\,{-2}$ and $d_C = 1\,\mathrm{e}\,{-6}$.

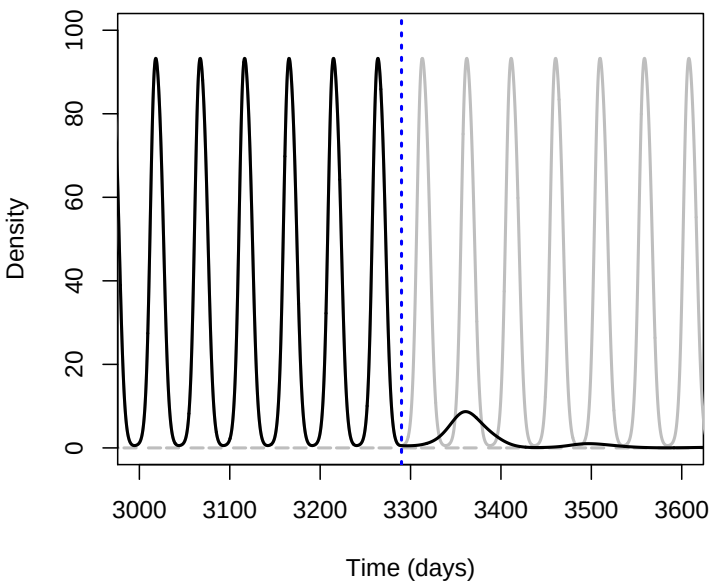

Fig. S15. Asymptotic moth dynamics predicted at 9°C (dashed tray line) and at 25°C (solid tray line). Transient dynamics (black line) are shown starting at the asymptotic dynamics of 25°C, with an abrupt change to 9°C at the blue line. Parameter estimates are given in Table S2 with $\gamma_C = 4\,\mathrm{e}\,{-2}$ and $d_C = 1\,\mathrm{e}\,{-6}$.

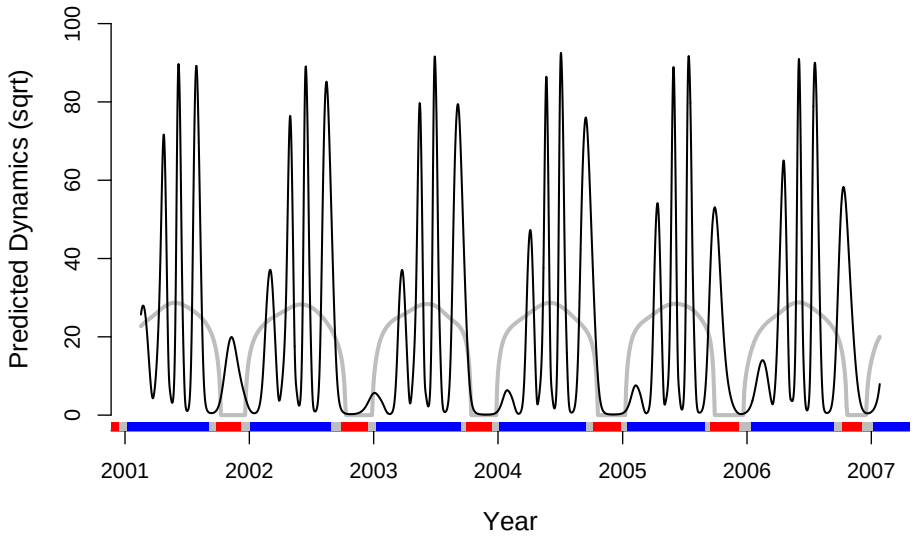

Fig. S16. Moth dynamics (black line) predicted from Kagoshima temperature dynamics. Equilibrium dynamics are shown in the coloured line, with non-persistent periods in red, stable equilibrium in gray, and unstable equilibrium (limit cycles) in blue. Parameter estimates are given in Table S2 with $\gamma_C = 4\,\mathrm{e}\,{-2}$ and $d_C = 1\,\mathrm{e}\,{-6}$.

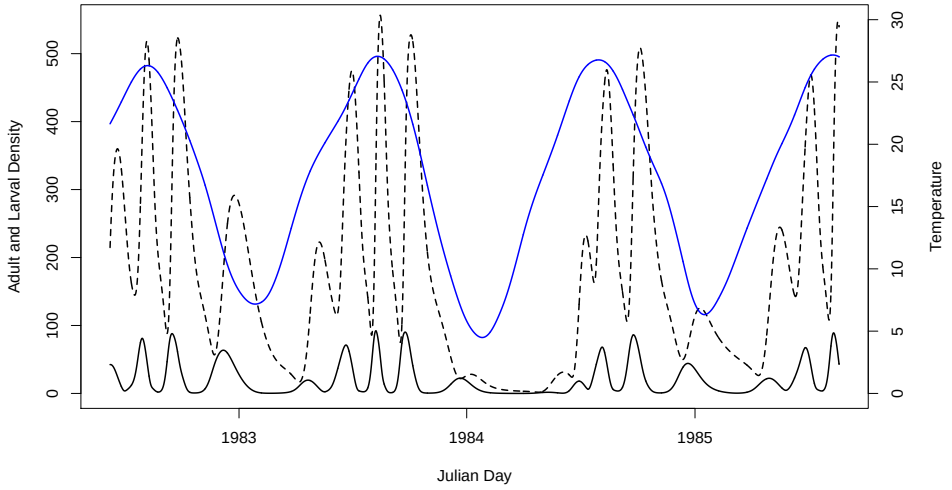

Fig. S17. Example larval (dashed black line) and adult (solid black line) dynamics predicted by the model driven with observed Kagoshima temperature dynamics. Temperature is shown on the secondary axis (blue line).

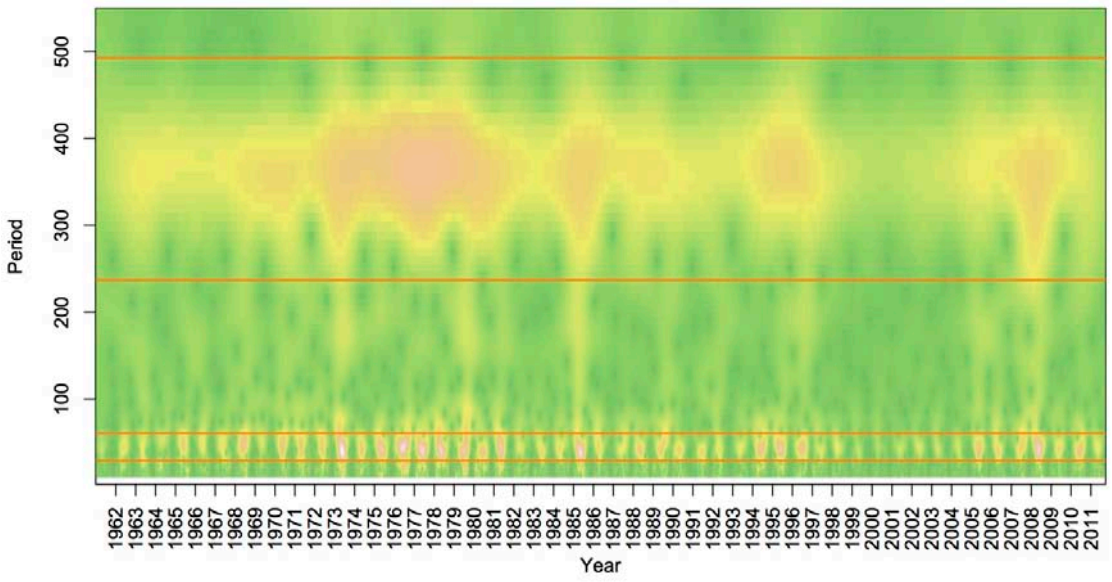

Fig. S18. Time-scale wavelet decomposition of the data in Fig. 1. Quality reconstruction of the time-series requires a high-resolution and wide period wavelet (no=15, nv=256). Horizontal lines delineate the two regions of reconstruction (Sub-annual period: $29 < \tau < 61$, Annual: $237 < \tau < 493$), and colours denote the square root of the wavelet power.

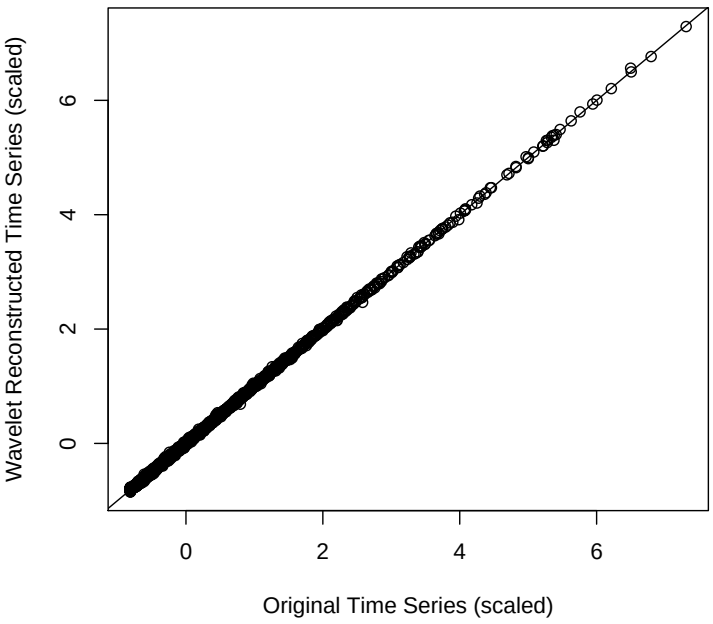

Fig. S19. Correlation between the original time-series and the wavelet reconstruction across all frequencies illustrating high quality in the time-series reconstruction. The solid line is the one-to-one relationship.

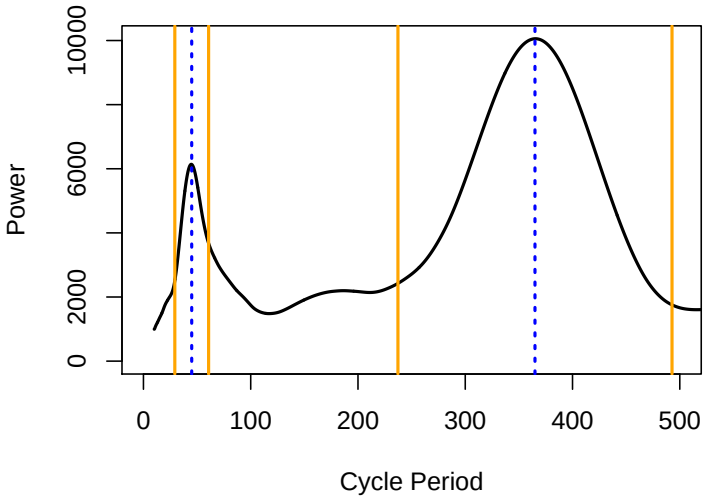

Fig. S20. Global power spectrum showing the dominant annual (τ=365 days) and sub-annual (τ=45 days) cycle (dashed blue lines) of the original time-series. Vertical orange lines denote the ±35% region used for reconstruction of annual and sub-annual cycles.

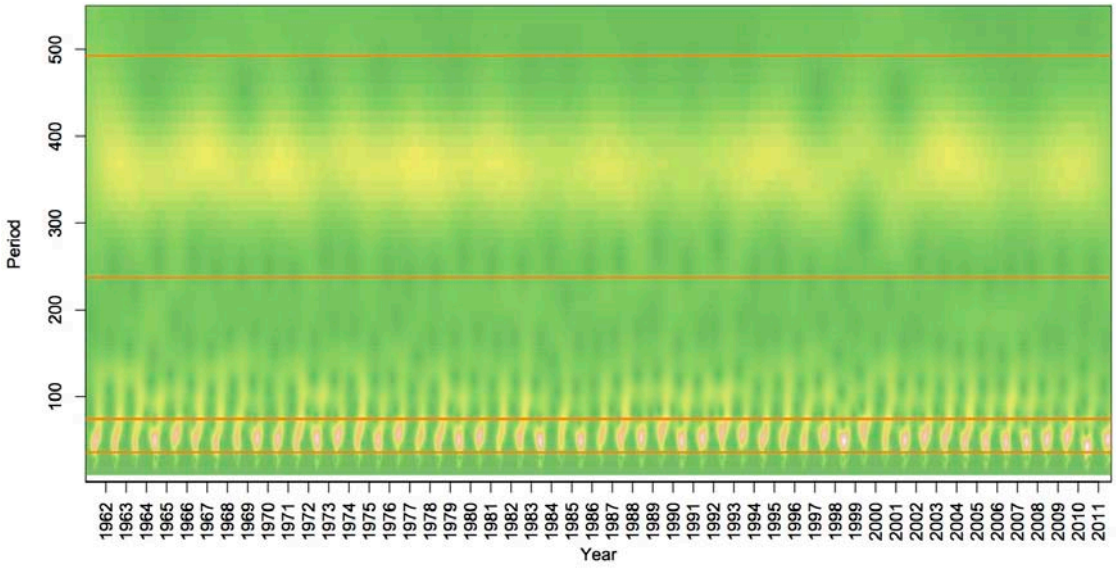

Fig. S21. Time-scale wavelet decomposition of the model predictions. Horizontal lines delineate the two regions of reconstruction (Sub-annual period: $36 < \tau < 74$, Annual: $237 < \tau < 493$), and colours denote the square root of the wavelet power.

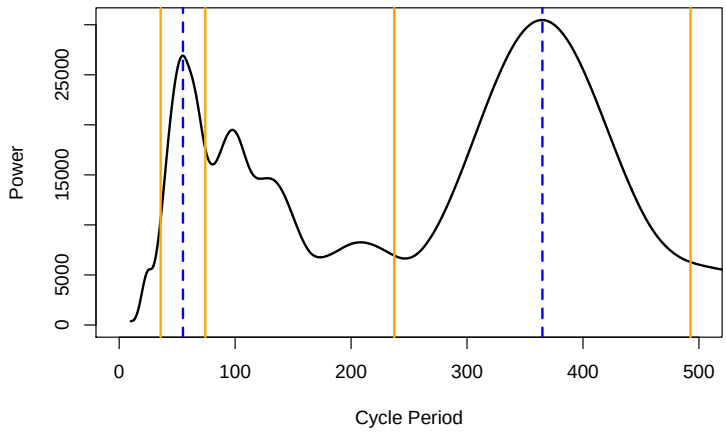

Fig. S22. Global power spectrum showing the dominant annual (τ=365 days) and sub-annual (τ=55 days) cycle (dashed blue lines) from the model predictions. Vertical orange lines denote the ±35% region used for reconstruction of annual and sub-annual cycles.

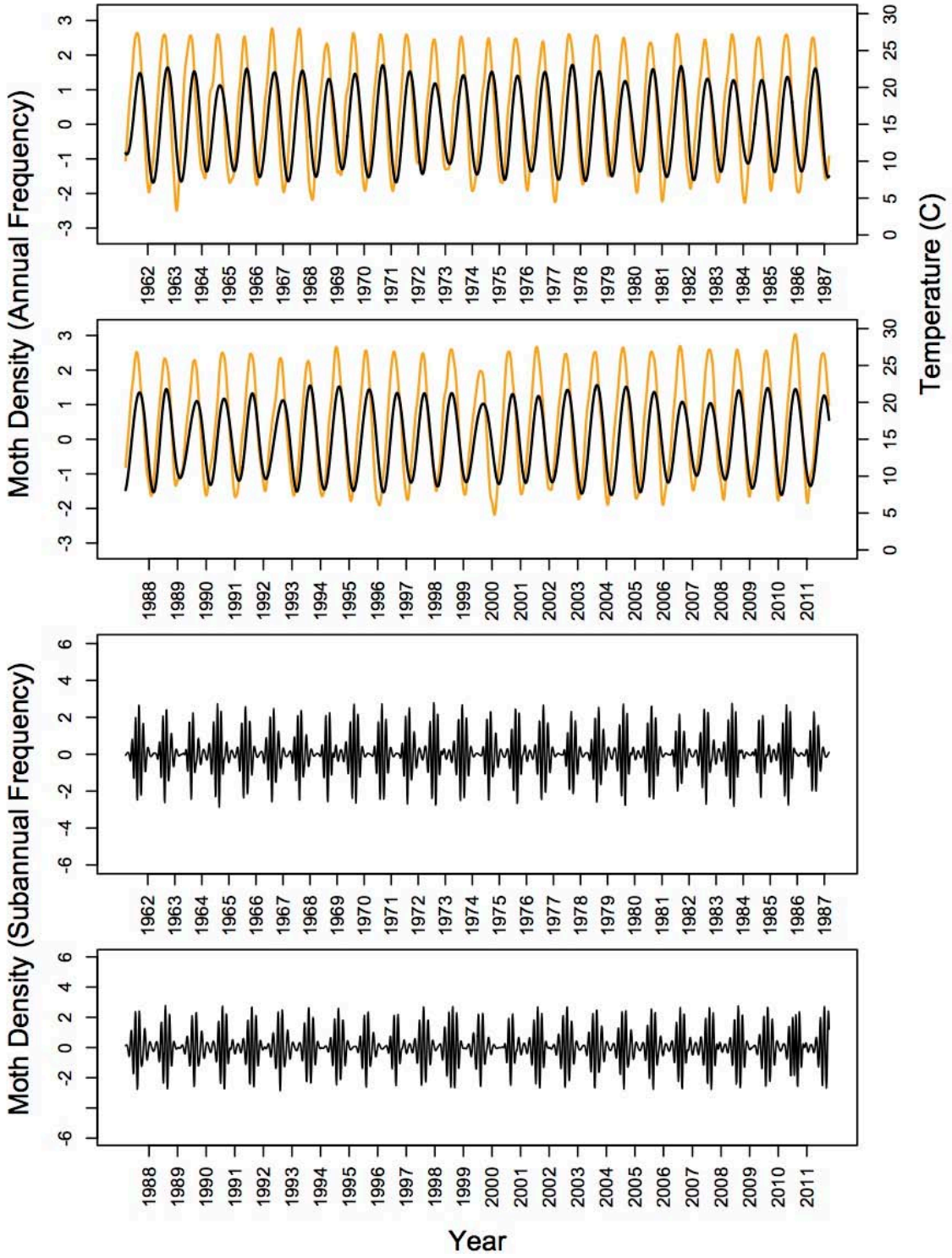

Fig. S23. Predicted changes in moth density (square root) at an annual frequency ($237 < \tau < 493$; upper two panels) and the sub annual frequencies ($36 < \tau < 74$; lower two panels). Scaled moth dynamics are shown with black lines, and smoothed temperature is shown with orange lines.

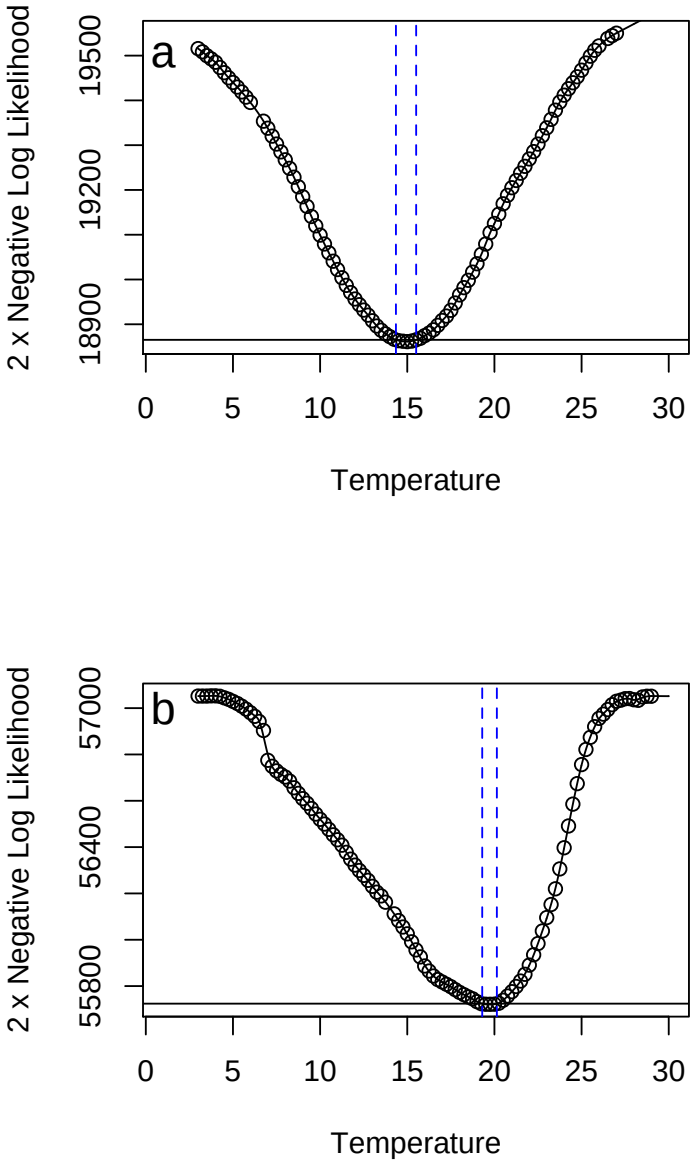

Fig. S24. Profile likelihood for the temperature threshold during the spring (a) and fall (b) phase. Horizontal line denotes the log-likelihood value for the 95% confidence intervals, and vertical blue lines show the temperature range for the interval.

Table S1.
Model selection for temperature dependence in life-history traits. Life-history functions have the general form $\alpha_x e^{\beta_x}$, where x denotes different possible levels of aggregation of stages and life-history traits. The data strongly support a separate α_{ij} for each stage (i) and each life-history trait (j). This table shows support for level of aggregation in the slope parameter β_x, and the best model suggests all traits and stages should share a common value. M1: different values of β for each trait but shared across stages. M2: different values of β for each stage in mortality. Other traits have their own value, but common across stages within those traits. M3: different values of β for each stage in mortality, but common across all other traits and stages. M4: birth and development share one value of β (common for all stages), but mortality has a different value (common for all stages). M5: mortality and birth share one value of β (common for all stages), but development has a different value (common for all stages). M6: mortality and development share one value of β (common for all stages), but birth has a different value.

α_{ij}	M0	M1	M2	M3	M4	M5	M6	df	AICc	ΔAICc
+	+	-	-	-	-	-	-	11	145.1	0
+	-	-	-	-	-	+	-	12	147.4	2.28
+	-	-	-	-	+	-	-	12	147.4	2.38
+	-	-	-	-	-	-	+	12	147.8	2.69
+	-	-	-	+	-	-	-	12	149.7	4.61
+	-	+	-	-	-	-	-	13	150.2	5.06
+	-	-	+	-	-	-	-	16	152.7	7.54

Table S2.
Parameter estimates based on laboratory data.

Parameter	Value	Description
β	$7.545e-2$	temperature exponent in development and birth rate functions
α_E	$1.200e-2$	scalar in egg development rate function
α_L	$7.311e-3$	scalar in larvae development rate function
α_P	$2.170e-2$	scalar in pupae development rate function
α_A	$1.295e-2$	scalar in adult development rate function
d_E	$4.953e-3$	scalar in egg mortality rate function
d_L	$1.195e-3$	scalar in larval mortality rate function
d_P	$4.333e-3$	scalar in pupal mortality rate function
d_A	$1.343e-2$	scalar in adult mortality rate function
b_0	5.688	scalar in birth rate function
β_W	$2.646e-1$	temperature exponent in winter mortality function
d_W	$5.614e-1$	temperature scalar in winter mortality function for larval stage
d_C	$-$	scalar for larval density dependence (no data so range explored)
γ_C	$-$	temperature exponent in larval competition rate function (no data so range explored)

References

1. J. F. Gillooly, J. H. Brown, G. B. West, V. M. Savage, E. L. Charnov, Effects of size and temperature on metabolic rate. *Science* **293**, 2248–2251 (2001). doi:10.1126/science.1061967 Medline

2. D. Atkinson, Temperature and organism size—a biological law for ectotherms? *Adv. Ecol. Res* **25**, 1–58 (1994). doi:10.1016/S0065-2504(08)60212-3

3. J. Forster, A. G. Hirst, G. Woodward, Growth and development rates have different thermal responses. *Am. Nat.* **178**, 668–678 (2011). doi:10.1086/662174 Medline

4. F. Taylor, Ecology and evolution of physiological time in insects. *Am. Nat.* **117**, 1 (1981). doi:10.1086/283683

5. M. J. Tauber, C. A. Tauber, S. Masaki, *Seasonal Adaptations of Insects* (Oxford Univ. Press, Oxford, 1986).

6. D. A. Roff, in *Diapause and Life Cycle Strategies in Insects* (Junk, The Hague, 1983), pp. 253–270.

7. H. V. Danks, *Insect Dormancy: An Ecological Perspective* [Biological Survey of Canada (Terrestrial Arthropods), Ottawa, 1987].

8. W. S. C. Gurney, P. H. Crowley, R. M. Nisbet, Stage-specific quiescence as a mechanism for synchronizing life-cycles to seasons. *Theor. Popul. Biol.* **46**, 319–343 (1994). doi:10.1006/tpbi.1994.1030

9. J. A. Powell, J. L. Jenkins, J. A. Logan, B. J. Bentz, Seasonal temperature alone can synchronize life cycles. *Bull. Math. Biol.* **62**, 977–998 (2000). doi:10.1006/bulm.2000.0192 Medline

10. D. A. Vasseur, K. S. McCann, A mechanistic approach for modeling temperature-dependent consumer-resource dynamics. *Am. Nat.* **166**, 184–198 (2005). doi:10.1086/431285 Medline

11. M. I. O'Connor, B. Gilbert, C. J. Brown, Theoretical predictions for how temperature affects the dynamics of interacting herbivores and plants. *Am. Nat.* **178**, 626–638 (2011). doi:10.1086/662171 Medline

12. S. Altizer, A. Dobson, P. Hosseini, P. Hudson, M. Pascual, P. Rohani, Seasonality and the dynamics of infectious diseases. *Ecol. Lett.* **9**, 467–484 (2006). doi:10.1111/j.1461-0248.2005.00879.x Medline

13. J. Ohlberger, E. Edeline, L. A. Vøllestad, N. C. Stenseth, D. Claessen, Temperature-driven regime shifts in the dynamics of size-structured populations. *Am. Nat.* **177**, 211–223 (2011). doi:10.1086/657925 Medline

14. Y. Tamaki, in *Tortricid Pests: Their Biology, Natural Enemies, and Control* (Elsevier, Amsterdam, 1991), pp. 541–551.

15. T. Yamanaka, W. A. Nelson, K. Uchimura, O. N. Bjørnstad, Generation separation in simple structured life cycles: Models and 48 years of field data on a tea tortrix moth. *Am. Nat.* **179**, 95–109 (2012). doi:10.1086/663201 Medline

16. T. M. Massie, B. Blasius, G. Weithoff, U. Gaedke, G. F. Fussmann, Cycles, phase synchronization, and entrainment in single-species phytoplankton populations. *Proc. Natl. Acad. Sci. U.S.A.* **107**, 4236–4241 (2010). doi:10.1073/pnas.0908725107 Medline

17. D. J. Lactin, N. J. Holliday, D. L. Johnson, R. Craigen, Improved rate model of temperature-dependent development by arthropods. *Environ. Entomol.* **24**, 68–75 (1995).

18. R. Carmona, W. L. Hwang, B. Torresani, *Practical Time-Frequency Analysis*, vol. 9, *Gabor and Wavelet Transforms, with an Implementation in S* (Academic Press, San Diego, CA, 1998).

19. W. W. Murdoch, B. E. Kendall, R. M. Nisbet, C. J. Briggs, E. McCauley, R. Bolser, Single-species models for many-species food webs. *Nature* **417**, 541–543 (2002). doi:10.1038/417541a Medline

20. N. C. Stenseth, W. Falck, O. N. Bjørnstad, C. J. Krebs, Population regulation in snowshoe hare and Canadian lynx: Asymmetric food web configurations between hare and the lynx. *Proc. Natl. Acad. Sci. U.S.A.* **94**, 5147–5152 (1997). doi:10.1073/pnas.94.10.5147 Medline

21. R. A. Taylor, A. White, J. A. Sherratt, How do variations in seasonality affect population cycles? *Proc.Biol. Soc. B* **280**, 20122714 (2013). doi:10.1098/rspb.2012.2714 Medline

22. S. Rinaldi, S. Muratori, Y. Kuznetsov, Multiple attractors, catastrophes, and chaos in seasonally perturbed predator-prey communities. *Bull. Math. Biol.* **55**, 15–35 (1993) doi:10.1016/S0092-8240(05)80060-6.

23. M. L. Rosenzweig, Paradox of enrichment: Destabilization of exploitation ecosystems in ecological time. *Science* **171**, 385–387 (1971). doi:10.1126/science.171.3969.385 Medline

24. A. Binzer, C. Guill, U. Brose, B. C. Rall, The dynamics of food chain under climate change and nutrient enrichment. *Philos. Trans. R. Soc. London B Biol. Sci.* **367**, 2935–2944 (2012). doi:10.1098/rstb.2012.0230 Medline

25. L. Becks, H. Arndt, Transitions from stable equilibria to chaos, and back, in an experimental food web. *Ecology* **89**, 3222–3226 (2008). doi:10.1890/07-1988.1

26. G. F. Fussmann, S. P. Ellner, K. W. Shertzer, N. G. Hairston Jr., Crossing the hopf bifurcation in a live predator-prey system. *Science* **290**, 1358–1360 (2000). doi:10.1126/science.290.5495.1358 Medline

27. E. McCauley, R. M. Nisbet, W. W. Murdoch, A. M. de Roos, W. S. C. Gurney, Large-amplitude cycles of *Daphnia* and its algal prey in enriched environments. *Nature* **402**, 653–656 (1999). doi:10.1038/45223

28. R. F. Costantino, J. M. Cushing, B. Dennis, R. A. Desharnais, Experimentally induced transitions in the dynamic behavior of insect populations. *Nature* **375**, 227–230 (1995). doi:10.1038/375227a0

29. D. M. Johnson, U. Büntgen, D. C. Frank, K. Kausrud, K. J. Haynes, A. M. Liebhold, J. Esper, N. C. Stenseth, Climatic warming disrupts recurrent Alpine insect outbreaks. *Proc. Natl. Acad. Sci. U.S.A.* **107**, 20576–20581 (2010). doi:10.1073/pnas.1010270107 Medline

30. T. Cornulier, N. G. Yoccoz, V. Bretagnolle, J. E. Brommer, A. Butet, F. Ecke, D. A. Elston, E. Framstad, H. Henttonen, B. Hörnfeldt, O. Huitu, C. Imholt, R. A. Ims, J. Jacob, B. Jędrzejewska, A. Millon, S. J. Petty, H. Pietiäinen, E. Tkadlec, K. Zub, X. Lambin, Europe-wide dampening of population cycles in keystone herbivores. *Science* **340**, 63–66 (2013). doi:10.1126/science.1228992

31. R. M. Nisbet, W. S. C. Gurney, The systematic formulation of population-models for insects with dynamically varying instar duration. *Theor. Popul. Biol.* **23**, 114–135 (1983). doi:10.1016/0040-5809(83)90008-4

32. F. H. Nabeta, M. Nakai, Y. Kunimi, Effects of temperature and photoperiod on the development and reproduction of *Adoxophyes honmai* (Lepidoptera: Tortricidae). *Appl. Entomol. Zool. (Jpn.)* **40**, 231–238 (2005). doi:10.1303/aez.2005.231

33. S. Kodomari, A. Tatara, Y. Kosugi, T. Nishijima, *Visual Guide of the Tea Pests and Pathogens: New Series* (Chamber of Tea Association of Shizuoka Prefecture, Shizuoka, 2003).

34. B. K. Byun, B.-W. Lee, E.-S. Lee, D.-S. Choi, Y. M. Park, C. Y. Yang, S. Lee, S. Cho, A review of the genus *Adoxophyes* (Lepidoptera Tortricidae) in Korea, with a description of *A. paraorana* sp. nov. *Anim. Cells Syst.* **16**, 154–161 (2012). doi:10.1080/19768354.2011.611175

35. P. G. Milonas, M. Savopoulou-Soultani, Development, survivorship and reproduction of *Adoxophyes orana* (Lepidoptera: Tortricidae) at constant temperatures. *Ann. Entomol. Soc. Am.* **93**, 96–102 (2000). doi:10.1603/0013-8746(2000)093[0096:DSAROA]2.0.CO;2

36. J. Régnière, J. Powell, B. Bentz, V. Nealis, Effects of temperature on development, survival and reproduction of insects: Experimental design, data analysis and modeling. *J. Insect Physiol.* **58**, 634–647 (2012). doi:10.1016/j.jinsphys.2012.01.010 Medline

37. H. M. Jo, Y. Kim, Relationship between cold hardiness and diapause in the smaller fruit tortrix, *Adoxophyes orana* (Fischer von Roslerstamm). *J. Asia Pac. Entomol.* **4**, 1–9 (2001). doi:10.1016/S1226-8615(08)60094-1

38. E. McCauley, W. A. Nelson, R. M. Nisbet, Small-amplitude cycles emerge from stage-structured interactions in *Daphnia*-algal systems. *Nature* **455**, 1240–1243 (2008). doi:10.1038/nature07220 Medline

39. K. Engelborghs, D. Roose, On stability of LMS methods and characteristic roots of delay differential equations. *SIAM J. Numer. Anal.* **40**, 629–650 (2002). doi:10.1137/S003614290037472X

40. R Development Core Team, *R: A Language and Environment for Statistical Computing* (R Foundation for Statistical Computing, Vienna, Austria, 2012); www.Rproject.org/.

41. C. Torrence, G. P. Compo, A practical guide to wavelet analysis. *Bull. Am. Meteorol. Soc.* **79**, 61–78 (1998). doi:10.1175/1520-0477(1998)079<0061:APGTWA>2.0.CO;2

42. J. Pinheiro, D. Bates, *Mixed-Effects Models in S and S-PLUS* (Springer, New York, 2000).